Utrecht University

Rijksinstituut voor Volksgezondheid
en Milieu
Ministerie van Volksgezondheid,
Welzijn en Sport

Modeling ozone Air Quality in the Netherlands and North-Western Europe in 2050

Thomas Eames

Supervisor: Prof. Dr. Ir. Guus Velders
2^{nd} Supervisor: Prof. Dr. Thomas Röckmann

Institute for Marine and Atmospheric Research (IMAU)
Utrecht University
The Netherlands
3 July 2018
Front Matter: Smog and haze in Central London

Abstract

Tropospheric ozone is a species whose concentration partially depends on meteorology, and partially on a complex non-linear chemistry. It is also hazardous to human health, and high ozone spikes in particular can be damaging to the respiratory and cardiovascular systems. Investigating the effect of climate change on ozone is a necessary aspect of any assessment of any future health impacts. This study aims to use two Representative Concentration Pathways (2.6 and 8.5) to quantify what changes in climate mean for ozone air quality and associated health effects in North-Western Europe. The WRF-Chem model is used, with a high resolution (6.6 x 6.6 km) domain nested in larger, lower-resolution pan-European parent domains.
Firstly, the methods of speciation for Non-Methane Volatile Organic Compounds, emissions & forcing input, boundary & initial conditions for the different scenarios are introduced. The model is then shown to have a general negative bias when considering ozone levels, most likely due to inconsistencies between the emissions dataset and fluctuations in local emissions on short timescales. This results in likely very conservative estimates Relative Risk to health as a result of ozone pollution in the model, but the risk can be shown to be increasing from 2010 to 2050. Shown also is that general ozone levels are less sensitive to climate changes directly but more so to Nitrogen Oxides ($NO_x = NO + NO_2$) concentrations, which themselves are influenced to a degree by meteorology.

Acronyms

AQD Air Quality Directive.

CBM-Z Carbon Bond Mechanism version Z.
CCSM4 Community Climate System Model 4.
CFSR Climate Forecast System Reanalysis.
CRMSE Correlation Root Mean Squared Error.

EC European Commission.
EDGAR Emissions Database for Global Atmospheric Research.
EEA European Environment Agency.
EMEP European Monitoring and Evaluation Programme.
ESRL Earth System Research Laboratory.
EU European Union.

FAIRMODE Forum for AIR quality MODelling in Europe.

GFS Global Forecast System.
GHG Greenhouse Gas.

IPCC Intergovernmental Panel on Climate Change.

LV Limit Value.

MOZART Model for OZone And Related chemical Tracers.
MPC Model Performance Criteria.
MPI Model Performance Indicator.
MQI Model Quality Indicator.
MQO Model Quality Objective.

NCAR National Center for Atmospheric Research.
NMVOC Non-Methane Volatile Organic Compound.
NOAA National Oceanic and Atmospheric Administration.

OECD Organisation for Economic Co-operation and Development.

PAN Peroxyacyl Nitrate.

RADM2 Regional Acid Deposition Model 2.
RCP Representative Concentration Pathway.
RIVM National Institute for Public Health and the Environment (Netherlands).
RMS$_U$ Root Mean Squared Uncertainty.
RMSE Root Mean Squared Error.
RR Relative Risk.
RRTM Rapid Radiative Transfer Model.
RRTMG Rapid Radiative Transfer Model for General circulation models.

SNAP Standardised Nomenclature for Air Pollutants.
SST Sea Surface Temperature.

VOC Volatile Organic Compound.

WHO World Health Organisation.
WRF-Chem Weather Research & Forecasting model with coupled online chemistry.

Contents

0 Introduction

Air pollution is a problem in European and north American cities, ozone pollution in particular being on the rise in many urban locations and to varying degrees in rural regions too. Frequent violations of air quality guidelines set by the European Union (EU) and the World Health Organisation (WHO) occur in most of Europe's urban areas. As surface ozone is sensitive to both the meteorology and chemistry of the troposphere, a changing climate may result in a more drastic change in ozone levels than anticipated. It is the goal of this study to investigate ozone in connection with climate change, with regard to two Representative Concentration Pathways (RCPs) for the year 2050 - RCP 2.6 for lower forcing scenario and RCP 8.5 for a higher forcing scenario. The degree of influence of meteorology and anthropogenic emissions will also be examined. The following research questions will be addressed:

1. How does ozone change with changing climate?
2. Are ozone spikes more sensitive to anthropogenic emissions or meteorology in a future climate?
3. What is the risk to human health?

To answer these questions, the Weather Research & Forecasting model with coupled online chemistry (WRF-Chem) will be employed, and several simulations will be performed pertaining to the different scenarios. Previous studies done for the USA (Penrod et al. (2014), Jacob and Winner (2009), Tagaris et al. (2007) and Hogrefe et al. (2004)) show differing results for different types of ozone in summer - background levels decrease with climate change, but ozone pollution (i.e. ozone formed from precursors with anthropogenic origins) exhibits the opposite trend and Penrod et al. (2014) found that effects from changes in anthropogenic emissions dominate over changes in climate. A synthesis of several modeling studies investigating ozone sensitivity to climate change found a general positive trend in the summer months for ca. 2050 (Weaver et al., 2009) across the USA but differences between models in regional patterns due to differences in projected meteorology (insolation, temperature etc) and isoprene-nitrate chemistry parameterisation. Most of these studies in the synthesis report daily 8-hour maximum ozone changes on the order of 0 to +10 ppb ($<$20 μg m^{-3}).

In the first section of this report the background to the problem will be introduced, including a description of the non-linear chemistry and aspects of local/regional meteorology which govern tropospheric ozone. In the following section the model will be briefly introduced and a detailed description given of the set-up for each model run. After this has been done the model performance will be evaluated with respect to observational data from the AirBase network. Finally, results will be presented and analysed, with the last section kept for discussion and any conclusions drawn.

1 Air Quality

Every year, 4.2 million deaths globally can be attributed to ambient air pollution (WHO, 2018). Air pollution will be, by 2050, the largest environmental cause of premature death (OECD, 2012) among Organisation for Economic Co-operation and Development (OECD) countries unless action is taken. Ozone is second only to particulate matter as the most serious air quality problem in Europe and, despite efforts to achieve cleaner air, many people live in areas where the air quality guidelines are regularly exceeded (EEA, 2011 - also see appendix). In 2014, 7% of Europe's urban population was exposed to ozone levels exceeding the EU limit (i.e. 8-hour mean concentrations above 120 μg m^{-3} for more than 25 days per year - see table 1) but 96% were living in areas where the WHO guideline was exceeded. The situation in 2015 was similar for the stricter WHO guideline (95%) but 30% lived in areas which exceeded the EU guideline (EEA, 2017). 2015 was the hottest European year on record (2017 likely exceeded this but at the time of writing there is no comprehensive ozone data available for this year). In the years preceding 2014 the population exposed to ozone concentrations exceeding the limit gradually decreased in line with EU emission reduction goals, but it seems likely that increasing temperature (and other related meteorological quantities) is related to higher ozone spikes.
The weather conditions that influence ozone concentrations are projected to change in the coming decades along with a changing climate. Assessing the extend of the risk to human health due to ozone in the future must then take into account changing weather conditions with changing radiative forcing, along with any emissions changes.

1.1 Health effects

Ozone exposure, both short (day-scale) and long (year-scale) term, can cause adverse health effects in human beings. Ozone is a powerful oxidant and can affect a wide range of biological material, in humans mostly tissues in the respiratory tract or lung (Beck et al., 1998). However, whilst elevated levels of ozone are associated with larger numbers of hospital admissions for respiratory complaints, a more significant effect on cardiovascular mortality is noted in Europe, with respiratory mortality not contributing significantly to the total number of ozone-related deaths (Katsouyanni et al., 2009).

	EU	WHO
Maximum daily 8-hour mean	120 μg m^{-3}	100 μg m^{-3}
Permitted exceedances	25 days per year	None

Table 1: Target and guideline values from the EU (EC, 2017) and WHO (WHO, 2005) respectively for ozone concentrations.

Table 1 shows the limit values as set by the EU and WHO, and also the number of times this value may be exceeded in a given period. The WHO lowered its guideline value in 2005, citing small but convincing amounts of evidence linking daily mortality and ozone levels below the previous guideline still maintained by the EU. The EU maintains a less stringent guideline with a number of permitted exceedances per year. However, evidence presented in WHO (2013) suggests that risk to human health begins already with concentrations above 70 μg m^{-3}, and for every 10 μg m^{-3} increment rise over a baseline of 70 μg m^{-3} increases daily mortality in ozone-related deaths by 0.3 - 0.5 %. On the basis of this

evidence then a concentration above the WHO guideline would already result in increased daily ozone mortality of 1-2 %.

Another way of quantifying this is by using Relative Risk (RR), as used by the World Health Organisation (WHO, 2013). The definition of RR used in this thesis is of an 'incidence ratio', i.e. "the incidence rate of disease occurrence in the exposed group divided by the incidence rate of disease occurrence in the unexposed group" (Tripepi et al., 2007).

$$RR = \frac{\text{Number of occurrences in exposed group}}{\text{Number of occurrences in unexposed group}} \tag{1.1}$$

For every 10 μg m^{-3} increase over 70 μg m^{-3} the RR of all-cause mortality attributed to ozone is 1.0029 (95% confidence interval 1.0014 - 1.0043). This is the measure which will be used in this thesis to investigate the effect of projected climate change on human health, with respect to ozone concentrations.

1.2 Chemistry

Many factors influence the surface level concentration of Ozone, as laid out in Seinfeld and Pandis, (1998). Ozone has a number of precursor species which form an interdependent reaction chain influenced by anthropogenic and biogenic emissions and meteorological factors, shown in figure 2. This makes reduction of ozone in the lower troposphere more complex than simply reducing emissions of the precursor gases.
The upper cycle in figure 2 between NO_2 and O_3 via NO and sunlight is the primary production method of ozone in the troposphere and is described in section 1.2.1. The red arrow pointing downwards from ozone shows its photolytic destruction, to form hydroxyl radicals, described in section 1.2.2. Two pathways are available for the OH radical - either a reaction with carbon monoxide to produce a hydroperoxyl radical (section 1.2.3) or with methane or another Non-Methane Volatile Organic Compound (NMVOC), producing another member of the peroxy radical family (section 1.2.4). These carbon-containing compounds are to a large extent controlled by surface emissions, marking part of the influence that anthropogenic activity (along with biomass burning and biogenic NMVOC emission) has on the ozone cycle with straight navy blue arrows. The other part of anthropogenic influence on the ozone cycle acts on peroxy radical reactions with NO, NO being heavily influenced by traffic emissions and higher up in the atmosphere by lightning events and aircraft emissions. The oxidation of NO via peroxy radicals to form NO_2 marks the closing of the extended cycle. The ratio of NO_x (the chemical family representing the sum of NO and NO_2) to NMVOC emissions is also important in determining ozone production rates and this is discussed in section 1.2.6. The small sub-cycle of formaldehyde on the left is also described in 1.2.5. As a final note, the transport of NO_x pollution to 'pristine' environments, and subsequent influence on the ozone cycle, is described in 1.2.7.

1.2.1 NO_x

The basic formation of ozone is dependent only on availability of NO_x and sunlight. Nitrogen dioxide is photolysed at wavelengths less than 424 nm to form nitrogen monoxide and a single oxygen atom. This atom reacts with an oxygen molecule (and a third molecule represented by M, which serves to remove excess energy from the reaction) to form ozone.

$$NO_2 + h\nu \rightarrow NO + O \tag{1.2a}$$
$$O + O_2 + M \rightarrow O_3 + M \tag{1.2b}$$

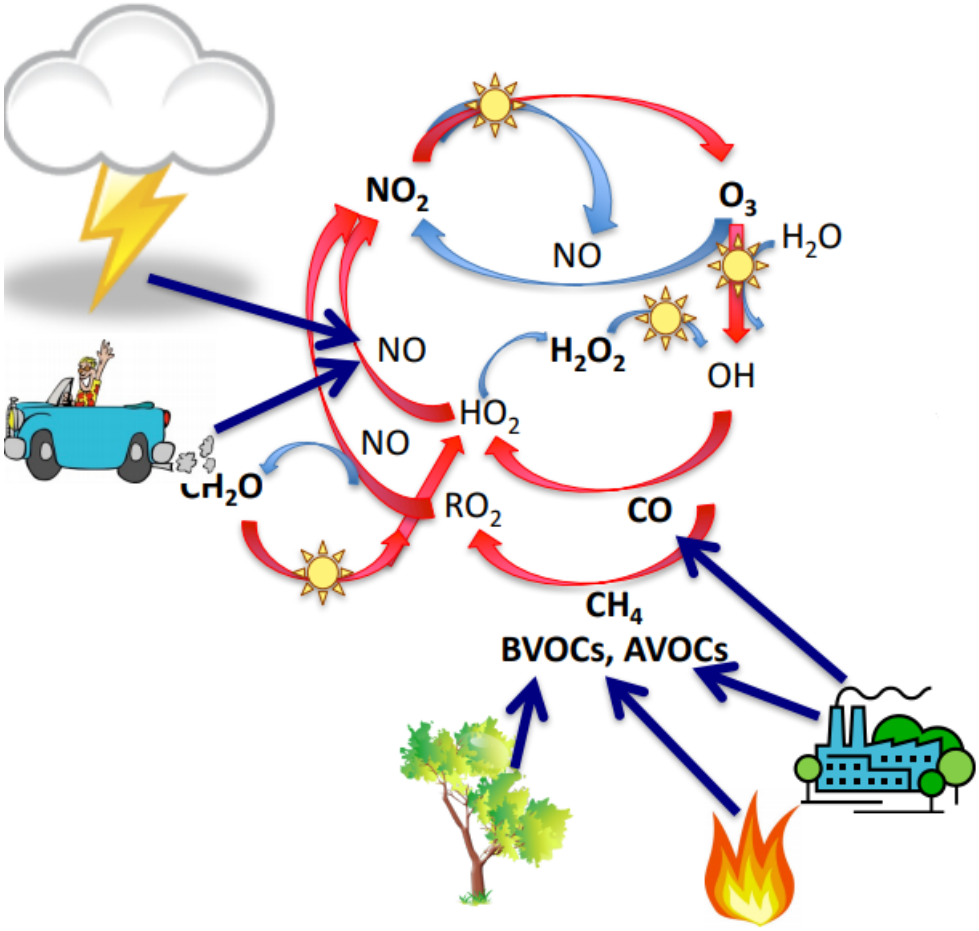

Figure 2: Tropospheric ozone chemistry diagram, taken from Bela et al. (2017). Shown with straight dark blue arrows are external emissions of various compounds from anthropogenic, biogenic and natural sources which play a role in the ozone cycle in the lower atmosphere.

The reaction chain is then closed by the reaction of the produced NO molecule with ozone. This is a primary removal pathway of tropospheric ozone and is known as NO_x titration.

$$O_3 + NO \rightarrow NO_2 + O_2 \tag{1.3}$$

Reactions (1.2) & (1.3) can be summarised neatly as an equilibrium reaction in the form of

$$NO_2 \overset{h\nu}{\rightleftharpoons} NO + O_3 \tag{1.4}$$

The mixing ratios of O_3 as calculated from this reaction chain underestimate the values obtained from measurements in many areas that are not considered 'remote', i.e. in or nearby urban areas, or in reasonably densely populated regions. In these areas, the other species previously mentioned also play a role in ozone formation.

1.2.2 Hydroxyl radical

Ozone can also be removed via photolysis and reaction with water vapour, abundant in the lower atmosphere. This reaction produces the hydroxyl radical, OH· (from here on, the

dot will indicate a radical species), which is a major reactant with respect to trace gases and plays an important role in incorporating other species (carbon monoxide, methane, and other NMVOCs) into the ozone reaction chain. Importantly, OH· is also unreactive to the main constituents of the atmosphere (N_2, O_2 etc).

$$O_3 + h\nu \rightarrow O + O_2 \tag{1.5a}$$
$$\rightarrow O(^1D) + O_2 \tag{1.5b}$$

The first branch produces a ground state oxygen atom - this is effectively a null cycle as this atom recombines with an oxygen molecule very quickly to produce ozone via (1.2b). In the lower troposphere where more water vapour is present $O(^1D)$ can react herewith to form the hydroxyl radical. Most often $O(^1D)$ will simply de-excite upon collision with another molecule, but up to 10% of $O(^1D)$ produced in (1.5b) can form OH·.

$$O(^1D) + M \rightarrow O + M \qquad (90\%) \tag{1.6a}$$
$$O(^1D) + H_2O \rightarrow 2\,OH\cdot \qquad (10\%) \tag{1.6b}$$

OH· can also be produced via photolysis of H_2O_2, which itself is formed via self-reaction of the hydroperoxyl radical (which is a product of carbon-containing species and OH· and will be discussed further later in this chapter).

$$HO_2 + HO_2 \rightarrow H_2O_2 + O_2 \tag{1.7a}$$
$$H_2O_2 + h\nu \rightarrow 2\,OH\cdot \tag{1.7b}$$

1.2.3 Carbon Monoxide

Carbon containing species are another major class of tropospheric compound which influence ozone levels. Carbon dioxide is a stable, longer lived species and does not play a significant role in ozone formation in the lower troposphere. Carbon monoxide, however, does. It is oxidised by OH· to form CO_2 and a hydrogen atom, continuing the chain shown on the right-hand side of figure 2 from photolysis of ozone as described in 1.2.2. The hydrogen atom combines fast enough with oxygen to form the hydroperoxyl radical that we can write it in one equation:

$$CO + OH\cdot \xrightarrow{O_2} CO_2 + HO_2\cdot \tag{1.8}$$

The hydroperoxyl radical is also very reactive and readily oxidises NO.

$$NO + HO_2\cdot \rightarrow NO_2 + OH\cdot \tag{1.9}$$

The net effect in comination with (1.2) is:

$$CO + 2\,O_2 + h\nu \rightarrow CO_2 + O_3 \tag{1.10}$$

Equation (1.9) is an analogue of (1.3) - the hydroperoxyl radical takes the place of ozone, and thus ozone is not removed by (1.3) and remains in the atmosphere, with the effect of an increase in ozone levels. This can be represented by a modification to (1.4), showing that NO is oxidised back into NO_2 via hydroperoxyl. In fact, during the process of oxidising NO the hydroperoxyl is itself converted to hydroxyl and then back via (1.8). This is a slower cycle, and the overall effect is thus the slow conversion of NO to NO_2 and modification of the ratio within NO_x family, and also an indirect effect on ozone concentrations.

$$NO_2 \overset{h\nu}{\rightleftharpoons} NO + O_3 \tag{1.11}$$

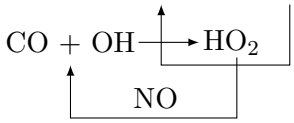

So in the presence of both CO and NO, more ozone is produced in the lower troposphere. Within the chain OH· is recycled, so without a sink the chain could continue indefinitely. In this case the sink is nitric acid (termination of the chain can also proceed via a self-reaction of hydroperoxyl but in the lower troposphere NO_x concentrations are such that this branch is not favoured).

$$OH\cdot + NO_2 + M \rightarrow HNO_3 + M \tag{1.12}$$

Nitric acid is then removed from the atmosphere via wet deposition, which is often in the form of acid rain.

1.2.4 Methane and other NMVOCs

Volatile Organic Compounds (VOCs) in the troposphere are also oxidised by the hydroxyl radical (produced via (1.5b) and (1.6)). Analagously with the case discussed in section 1.2.3, an organic compound can react with OH· to produce water and another radical (e.g. in the case of methane the methyl radical, $CH_3\cdot$, is produced), which then reacts almost instantaneously with O_2 to make the corresponding peroxy radical (using methane again as an example, the methyl peroxy radical $CH_3O_2\cdot$ is formed). In general terms this can be written as

$$RH + OH\cdot \xrightarrow{O_2} RO_2\cdot + H_2O \tag{1.13}$$

where R represents a generic hydrocarbon chain.
Again, following a similar path to the hydroperoxyl radical in the carbon monoxide chain, the organic peroxy molecule reacts with NO to form another organic compound and nitrogen dioxide. The organic molecule created can react fast with oxygen to form a secondary organic (for methane, the intermediate organic is the methoxy radical, $CH_3O\cdot$, and secondary organic is formaldehyde, HCHO).

$$RO_2\cdot + NO \xrightarrow{O_2} \textit{secondary}\,VOC + HO_2\cdot + NO_2 \tag{1.14}$$

In addition, the peroxyl radical produced can also react with hydroperoxyl, in direct competition with NO - this is also important for ozone levels because not only the abundance of NO_x and VOCs affect O_3 concentration, but also the ratio of these two species.

$$RO_2\cdot + HO_2\cdot \rightarrow ROOH + O_2 \tag{1.15}$$

1.2.5 Formaldehyde

Formaldehyde itself has a reaction chain which is interesting to consider in the context of ozone production, as CO is formed as an end product. It can be photolysed into a hydrogen atom (which as noted in 1.2.3 reacts very fast with oxygen to form hydroperoxyl) and HCO, which itself reacts quickly with O_2, forming $HO_2\cdot$ and CO.

$$HCO + O_2 \rightarrow HO_2\cdot + CO \tag{1.16}$$

Alternatively, HCHO reacts with the hydroxyl radical with HCO and H_2O as products, and HCO again rapidly reacts as in (1.16). The formaldehyde reaction chain can then be written as:

$$\mathrm{HCHO} + \mathrm{h}\nu \xrightarrow{\mathrm{O_2}} 2\,\mathrm{HO_2}\cdot + \mathrm{CO} \tag{1.17a}$$

$$\rightarrow \mathrm{H_2} + \mathrm{CO} \tag{1.17b}$$

$$\mathrm{HCHO} + \mathrm{OH}\cdot \xrightarrow{\mathrm{O_2}} \mathrm{HO_2}\cdot + \mathrm{CO} + \mathrm{H_2O} \tag{1.17c}$$

In direct overhead sunlight, the ratio of (1.17a) to (1.17b) is approximately 45% to 55% (Rogers, 1990). In this reaction chain therefore, it is reasonable to say that one formaldehyde molecule leads to approximately one hydroperoxyl radical.

1.2.6 VOC/NO_x ratio

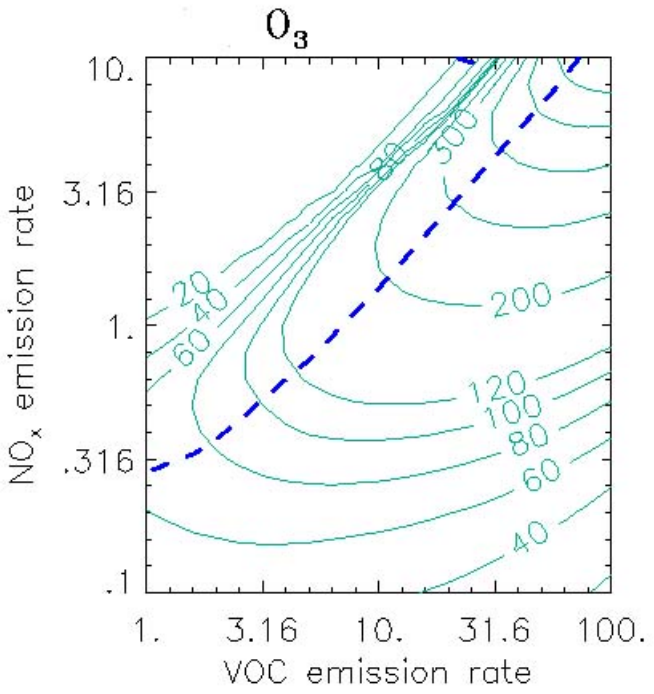

Figure 3: Ozone isopleths (ppb) as a function of VOC and NO_x emission rates, in 10^{12} molec $m^{-2}s^{-1}$. The isopleths (solid green lines) represent conditions during the afternoon following 3-day calculations with a constant emission rate, at the hour corresponding to maximum O3. The blue dashed line represents the transition from VOC-sensitive to NO_x-sensitive conditions. From Sillman and He, 2002.

The more complex nature of the tropospheric ozone reaction chain means that ozone concentrations are not linearly dependent on the concentrations of the precursor species named in the previous section. The O_3 concentration is determined in part by the ratio of VOCs to NO_x (shown in figure 3). To give a better understanding of the sensitivity of ozone to VOCs and NO_x, the chemistry laid out in the preceeding subsection can be summarised as follows (von Scheidemesser et al., 2015 and Sillman, 2003):

$$\mathrm{VOC} + \mathrm{OH} \xrightarrow{\mathrm{O_2}} \mathrm{RO_2} + \mathrm{H_2O} \tag{1.18a}$$

$$\mathrm{CO} + \mathrm{OH} \xrightarrow{\mathrm{O_2}} \mathrm{HO_2} + \mathrm{CO_2} \tag{1.18b}$$

$$\mathrm{RO_2} + \mathrm{NO} \xrightarrow{\mathrm{O_2}} \text{secondary VOC} + \mathrm{HO_2} + \mathrm{NO_2} \tag{1.18c}$$

$$\mathrm{HO_2} + \mathrm{NO} \rightarrow \mathrm{OH} + \mathrm{NO_2} \tag{1.18d}$$

$$\mathrm{NO_2} + \mathrm{h}\nu \rightarrow \mathrm{NO} + \mathrm{O} \tag{1.18e}$$

$$\mathrm{O} + \mathrm{O_2} + \mathrm{M} \rightarrow \mathrm{O_3} + \mathrm{M} \tag{1.18f}$$

The split between 'NO_x-sensitive' (VOC-saturated; the area to the right of the VOC:NO_x = 8:1 line in figure 3) and 'NO_x-saturated' (VOC-sensitive; area to the left of the line) is heavily dependent on the hydrogen radicals OH· and HO_2·. The radical chemistry has already been discussed previously: radical production proceeds via (1.5) - (1.6) and secondary VOC reactions (e.g. formaldehyde, as in (1.17)), and destruction via (1.12), (1.15) and the hydroperoxyl self-reaction (1.7a).

NO_x-sensitive regimes occur when (1.7a) and (1.15) dominate (1.12). The background concentrations of peroxyl radicals (i.e. the species which replace ozone in the NO_x titration reaction (1.3) and allow it to build up) are then determined by the balance between (1.5)/(1.6) and (1.17)/(1.7a) - although as the rate of (1.7a) is quadratic in HO_2 peroxyl radicals will not be very sensitive to changing NO_x/VOC concentrations in this regime. Ozone production rates are then approximately equal to the rate of peroxyl radical reactions with NO, (1.18c) and (1.18d) (Sillman and He, 2002). This rate increases with increasing NO_x.

NO_x-saturated regimes occur in opposite circumstances; when (1.12) is the dominant hydrogen radical sink. OH levels are then determined by balancing the radical sources with (1.12), and ozone production rate is dependent on (1.18a) and (1.18b). This rate increases with increasing VOC levels, but decreases with increasing NO_x levels as NO_2 then competes with VOCs and CO for the peroxyl radical. Because of this, there can exist situations where reducing NO_x concentrations can lead to an increase in ozone levels. This is the regime in which most polluted cities exist (for 2010, London and Amsterdam had a VOC:NO_x emission ratio of 1:618 and 1:803 respectively according to the Emissions Database for Global Atmospheric Research (EDGAR), introduced in section 2.5).

1.2.7 PAN chemistry

As a result of reaction chains initiated by organic compounds such as aldehydes (see section 5.8 of Seinfeld and Pandis for more details), Peroxyacyl Nitrate (PAN) (also known as acyl peroxy nitrate, APN) can be formed in the thermal equilibrium between nitrogen dioxide and organic peroxy radicals (Thornton, 2007).

$$\mathrm{RC(O)OO}\cdot + \mathrm{NO_2} + \mathrm{M} \rightleftharpoons \mathrm{RC(O)OONO_2} + \mathrm{M} \tag{1.19}$$

The PAN class of compound is relatively insoluble, photochemically inert and has a slow reaction rate with OH (Seinfeld and Pandis, 1998), leading to a relatively long atmospheric lifetime. PANs will dissociate more readily at higher temperatures but their lifetime is long enough to enable them to be vented into higher reaches of the troposphere where it is colder. Lower temperatures dramatically increase the lifetime of PANs (Thornton, 2007), making them capable of transporting NO_x from polluted regions to 'pristine' environments upon subsidence, warming of the air mass and subsequent shift to the left of the equilibrium in (1.19). This is illustrated in figure 4.

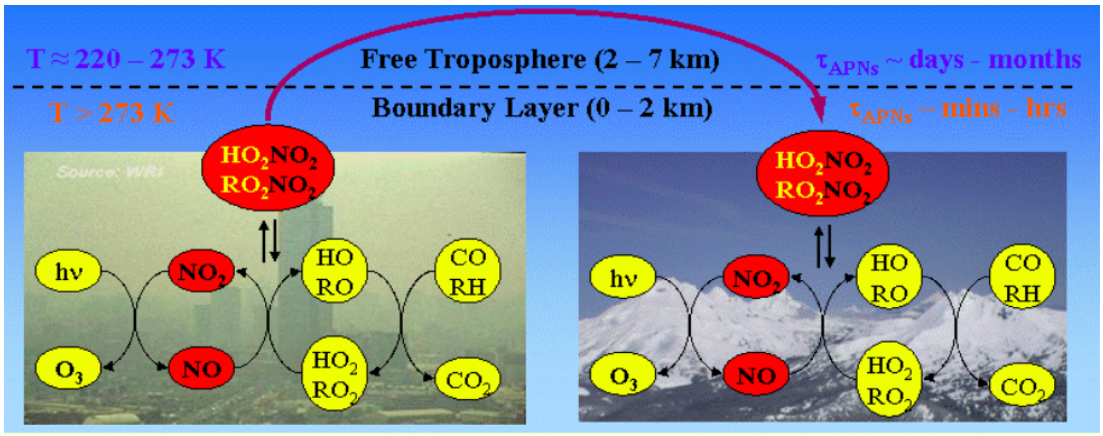

Figure 4: PAN transport of pollution to remote areas via venting and subsidence of air masses, and consequent feeding of the catalytic ozone cycle in an area with low anthropogenic pollution. Adapted from Thornton, 2007.

1.3 Meteorology

Atmospheric concentrations of trace gases and other species are not only affected by the chemistry of the layer but also by the prevailing meteorological conditions. Not only does this have to do with temperature affecting the chemistry or wind blowing species in/out of regions, but other weather conditions which can influence air quality.

1.3.1 Temperature

Higher ozone levels are associated with warmer temperatures (Wackter and Bayly (1988), Kelly et al. (1986), Sillman and Samson (1995)) for different reasons. Warmer temperatures can be an indicator of stagnant high-pressure weather systems (see section 1.3.2) but can also indirectly affect ozone concentrations via PAN chemistry (Seinfeld and Pandis, 1998 - see also section 1.2.7) and elevated tropospheric water vapour concentrations which can perturb OH (Ramanathan et al., 1987).
As the source of heat and light in our solar system, higher temperatures are also indicative of more solar input. This then feeds back to the chemistry, with a higher actinic flux accelerating photochemical reactions such as the production of ozone from nitrogen dioxide.
Increasing temperatures can also increase emissions of biogenic VOCs such as isoprene and monoterpenes (Guenther et al., 1991, Guenther et al., 1993) causing higher ozone concentrations in conditions that are not already VOC-saturated.

1.3.2 High Pressure systems

Another progenitor of high ozone levels are high-pressure weather systems (RTI, 1975). High pressure itself does not effect ozone concentrations but these systems provide favourable conditions for subsidence, weak winds and a cloud-free sky. Widespread subsidence in the troposphere creates stable boundary layer conditions due to the adiabatic warming of the sinking air, reducing the rate of convective mixing and potentially creating temperature inversions which serve as a lid keeping pollutants in the lower layer (NRC, 1991). Furthermore, subsidence reduces the planetary boundary layer height, increasing concentrations by virtue of the fact that the gases have a smaller volume to fill (Eshel and Bernstein, 2006).
The sinking and warming air masses also reduce the relative humidity in the region and makes cloud formation more unlikely (NRC, 1991 and Vallero, 2014), leading to more

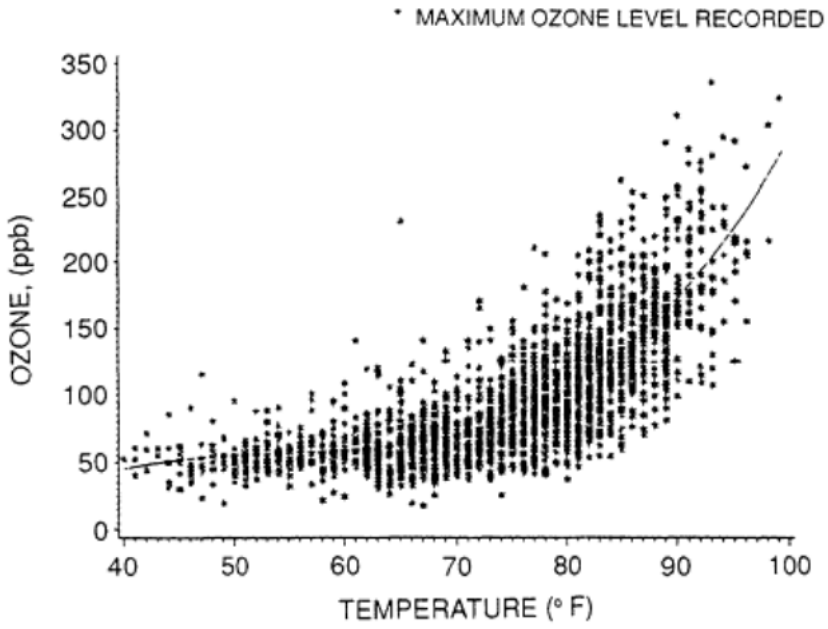

Figure 5: Daily maximum temperature plotted against maximum daily average ozone concentration in Connecticut, 1976 - 1986. From Wackter and Bayly, 1988.

favourable conditions for photochemical production. Fewer clouds also means less moist convection and venting into the upper troposphere, allowing for more extremes of ozone concentrations (Eshel and Bernstein, 2006).

1.3.3 Regional weather

In the study domain (north-western Europe) conditions favourable to high ozone spikes occur in stable atmospheric conditions, warm and dry weather with steady easterly winds. These easterlies also carry with them pollution from the east instead of relatively clean air from over the atlantic ocean, which can exacerbate the effect of the weather on ozone levels.
It is particularly the extent of these meteorological effects on ozone that this study intends to investigate and quantify.

2 Model set-up

In the following section the approach to the simulations is described. Initially an introduction to the model will be given, as well as an overview of the built-in options and choices made on how to run the model (sections 2.1 and 2.2). In sections 2.3 - 2.6, all the different inputs used in this study are described. In the final subsection, all the different simulations performed are listed.

2.1 Model description

This study uses the Weather Research & Forecasting model with coupled online chemistry (WRF-Chem) version 3.8.1, a fully compressible Euler non-hydrostatic mesoscale model. The coupled online chemistry accounts for interdependence of the meteorological and chemical processes (Grell et al., 2005). The model can be applied on different scales and explicitly solves meteorology instead of relying on prescribed fields, making it applicable for use in future projections on both meteorology and air quality. Table 2 shows the WRF-Chem setup for this study.

Parameterisations (WRF namelist option)	**Scheme** (namelist number)	**Reference**
Micro-Physics (mp_physics)	Lin et al. scheme (2)	Lin et al., 1983
Planetary Boundary Layer Physics (bl_pbl_physics)	Yonsei University Scheme (YSU) (1)	Hong et al., 2006
Cumulus Physics (cu_physics)	Grell-Freitas ensemble scheme (3)	Grell & Freitas, 2014
Short Wave Radiation (ra_sw_physics)	RRTMG scheme (4)	Iacono et al., 2008
Long Wave Radiation (ra_lw_physics)	RRTM scheme (1)	Mlawer et al., 1997
Land Surface option (sf_surface_physics)	Unified Noah Land-Surface Model (2)	Tewari et al., 2004
Chemistry mechanism (chem_opt)	CBM-Z mechanism (5)	Zaveri & Peters, 1999
Dry deposition (gas_drydep_opt)	Wesely scheme (1)	Wesely, 1989
Biogenic Emissions (bio_emiss_opt)	Guenther scheme (1)	Guenther et al., 1994, Simpson et al., 1995

Table 2: Different physics and chemistry options used for this study within WRF-Chem.

The long wave scheme is of particular relevance as, along with Sea Surface Temperature (SST) outputs for RCP 2.6 and 8.5, the radiative forcing is prescribed herein via concentrations of CO_2, N_2O and CH_4.

2.2 Model domains

This model consists of three domains, one parent and two nested within the parent domain. The parent domain (domain 1) is the European domain and has a coarse resolution

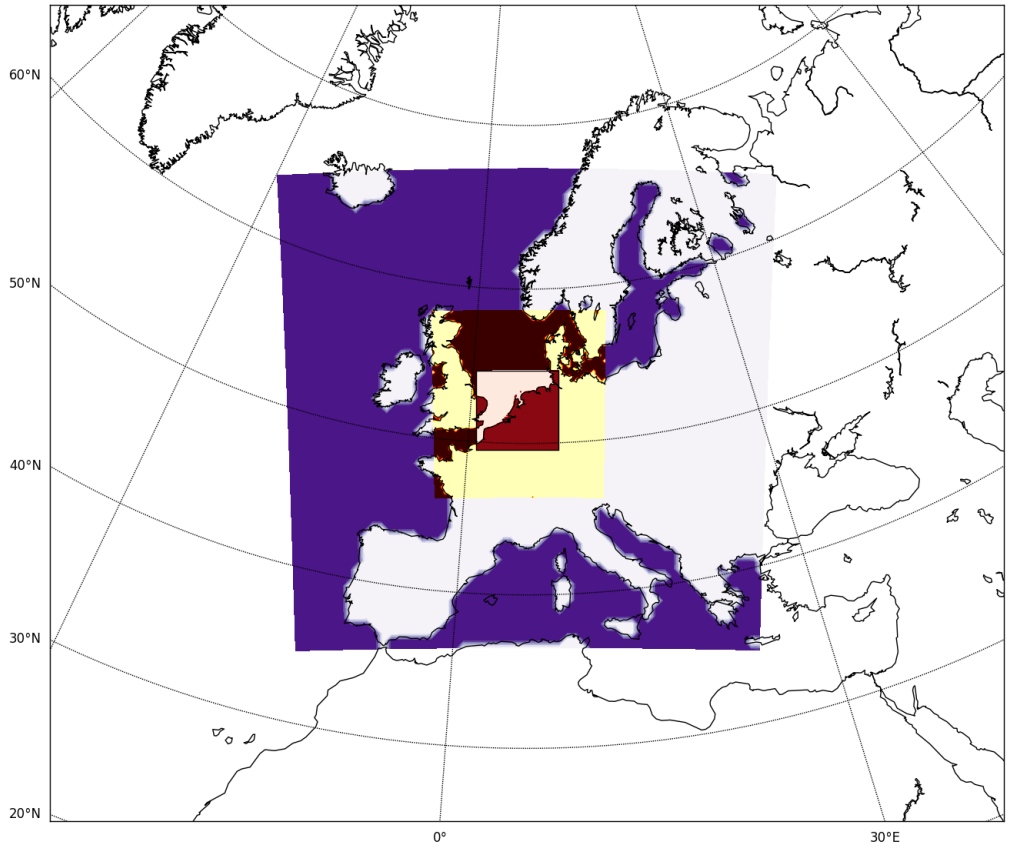

Figure 6: The parent domain and two nested domains used in this study.

of 60km x 60km - all external boundary conditions are applied to this domain. Nested within the first is a smaller, higher resolution domain (domain 2) covering most of north-western Europe, including most of Great Britain. This domain is 20km x 20km and takes its boundary conditions from domain 1. Finally, nested in domain 2 is the third domain, centred on the Netherlands and including all of the Benelux region as well as parts of France, England, Germany and Denmark. This domain is approximately 6km x 6km resolution (approximately as WRF-Chem does not work if the resolution difference is not kept to a factor of 3) and will be the domain of interest for this study. It takes boundary conditions from domain 2. The outer domains serve to calculate the meteorological boundary conditions for future scenarios, as these are not available.
Initially a higher resolution domain set was used (20x20km, approx. 6x6km and approx. 3x3km) but this proved to be problematic for the inputs - the WRF-Chem pre-processing system could not re-grid much coarser data onto this grid size. The domains are displayed in figure 6.

2.3 Boundary & Initial conditions

All meteorological boundary and initial conditions (save those mentioned in section 2.6 for RCP scenarios) are prescribed using the Global Forecast System (GFS) analysis 3 dataset

on a 1^o resolution. Sea Surface Temperatures for the 2010 runs are constrained with data from National Center for Atmospheric Research's Climate Forecast System Reanalysis (CFSR) dataset. Chemical initial & boundary conditions were provided by model output from Model for OZone And Related chemical Tracers (MOZART)-4, available from `http://www.acom.ucar.edu/wrf-chem/mozart.shtml`. Not all the MOZART-4 species have an equivalent within the CBM-Z chemistry scheme (see section 2.4) and most notably there are no fields for initial or boundary conditions of hydrocarbon groups HC3 or HC5 (see table 3), along with some other species such other members of the PAN family (e.g MPAN), or peracetic acid.

2.4 Chemistry parameterisation

The Carbon Bond Mechanism version Z (CBM-Z) Zaveri & Peters, 1999 is a lumped-structure mechanism, treating certain groups of organic species as one 'lump' according to the type of bond present. This is advantageous in terms of computational efficiency, and also conserves the carbon mass in the system. The disadvantage is that different species react at different rates and produce slightly different products, but the mechanism treats them as one species. It is therefore to be expected that non-linear cycles involving organics, such as the ozone cycle, are not completely accurate.

EDGAR/RCP	CBM-Z
Alcohols	E_CH3OH
	E_C2H5OH
Ethane	E_ETH
Propane	E_HC3
Butanes	
Ethyne	
Pentanes	E_HC5
Hexanes & higher alkanes	E_HC5
Ethene	E_OL2
Propene	E_OLT
Other alkenes & alkynes	E_OLI
Isoprene	E_ISO
Benzene	E_TOL
Toluene	
Other aromatics	
Xylene	E_XYL
Trimethylbenzenes	
Ethers	E_ALD
Other alkanals	
Formaldehyde	E_HCHO
Ketones	E_KET
Acetic acid and other higher acids	E_ORA2

Table 3: Mapping of species from EDGAR emissions data to the CBM-Z module. A total of 21 emitted species are mapped to 16 lumped species.

However, CBM-Z was used in the model preferentially over other mechanisms, such as the RADM2 mechanism (Stockwell et al., 1990), as it has been shown to better reproduce ozone levels over a European domain (Karlický et al., 2017). Dry deposition is also an important part of the ozone loss process in the atmosphere. Dry deposition is parameterised using the Wesely scheme, which takes into account surface conditions (e.g. dew, surface moisture, temperature) and plant stomatal response to these environmental conditions. Wet deposition is also taken into account in WRF-Chem version 3.8 (Grell & Ahmadov, 2016), although WRF-Chem appears to overpredict precipitation by roughly 25% every season (Karlický et al., 2017), potentially resulting in a negative bias in ozone over the modeled period.

2.5 Emissions parameterisation

The Emissions Database for Global Atmospheric Research (EDGAR) v4.3.1 (Crippa et al., 2016) was used to input the 'classic' pollutant emissions (NO_x, CO, SO_2, NH_3) and VOC emissions input was taken from v4.3.2 (Huang et al., 2017). The EDGAR emissions database was developed by the National Institute for Public Health and the Environment (Netherlands) (RIVM) in the 1990s and is maintained by the Joint Research Centre of the EC. Emissions are given in kg m^{-2} s^{-1} with a resolution of 0.1 x 0.1 degree and seperate datasets for (most) individual VOCs. Adaptions were necessary before this data could be used as input for WRF-Chem. The datasets are available as an annual average for each species, which is then adjusted for season (summer months) and time of day.
Emissions in a similar format to EDGAR were taken from the RCP Database (albeit with a somewhat coarser 1 x 1 degree resolution), for RCP 2.6 (van Vuuren et al., 2007) and 8.5 (Riahi et al., 2007). Methods used to parameterise emissions are similar for all emission sets and are described in sections 2.5.1 and 2.5.2. NO_x emissions from all datasets for the three different scenarios are shown as an example in figure 7. It is clear that resolution for the RCP scenarios is coarser than that of the EDGAR database (and this is true for all species), which will likely be at least part of the explanation for some localised differences between the scenarios (e.g. the influence of polluted cities in the RCP scenarios will be more dispersed than in the baseline scenario).

2.5.1 NO_x

Both NO and NO_2 are grouped into one species within the EDGAR database. Most NO_x is emitted in the form of NO, and NO_2 formed between 5-8% (PORG, 1997) of NO_x emissions, but this can depend on road traffic composition (e.g. increased use of catalytic converters or higher dependence on diesel engines). The percentage of NO_2 in NO_x emissions has been shown to be increasing (Carslaw, 2005). In this study therefore, it is assumed that NO_2 accounts for 10% and NO for the other 90% of total NO_x emissions.

2.5.2 VOCs

Due to the lumped-structure approach used in CBM-Z the individual VOC species or groups must be assigned to certain emission categories. Some species are directly mapped to their own CBM-Z category while others are lumped together within more general categories. How this is done is shown in table 3. Biogenic VOC emissions are considered separately, calculated online via the Guenther scheme (see table 2) based upon land use input, and temperature and photosynthetic active radiation calculated within the model.

2.5.3 Emission Profiles

Emissions input is entirely anthropogenic in nature, and as such is scaled with certain times of the day to reflect human activity. All model output will be evaluated against global background concentrations, so no one emissions category will be considered more important than another. The profile used (and different profiles for individual emissions categories) was taken from the European Monitoring and Evaluation Programme (EMEP) 2016 status report and are shown in figure 8.

2.6 Forcing parameterisation

Radiative forcing is the overarching factor that changes our climate, so in order to simulate changes in ozone the changes in forcing according to different RCP scenarios (2.6 and 8.5) must be parameterised in the model. There are two components of forcing that are

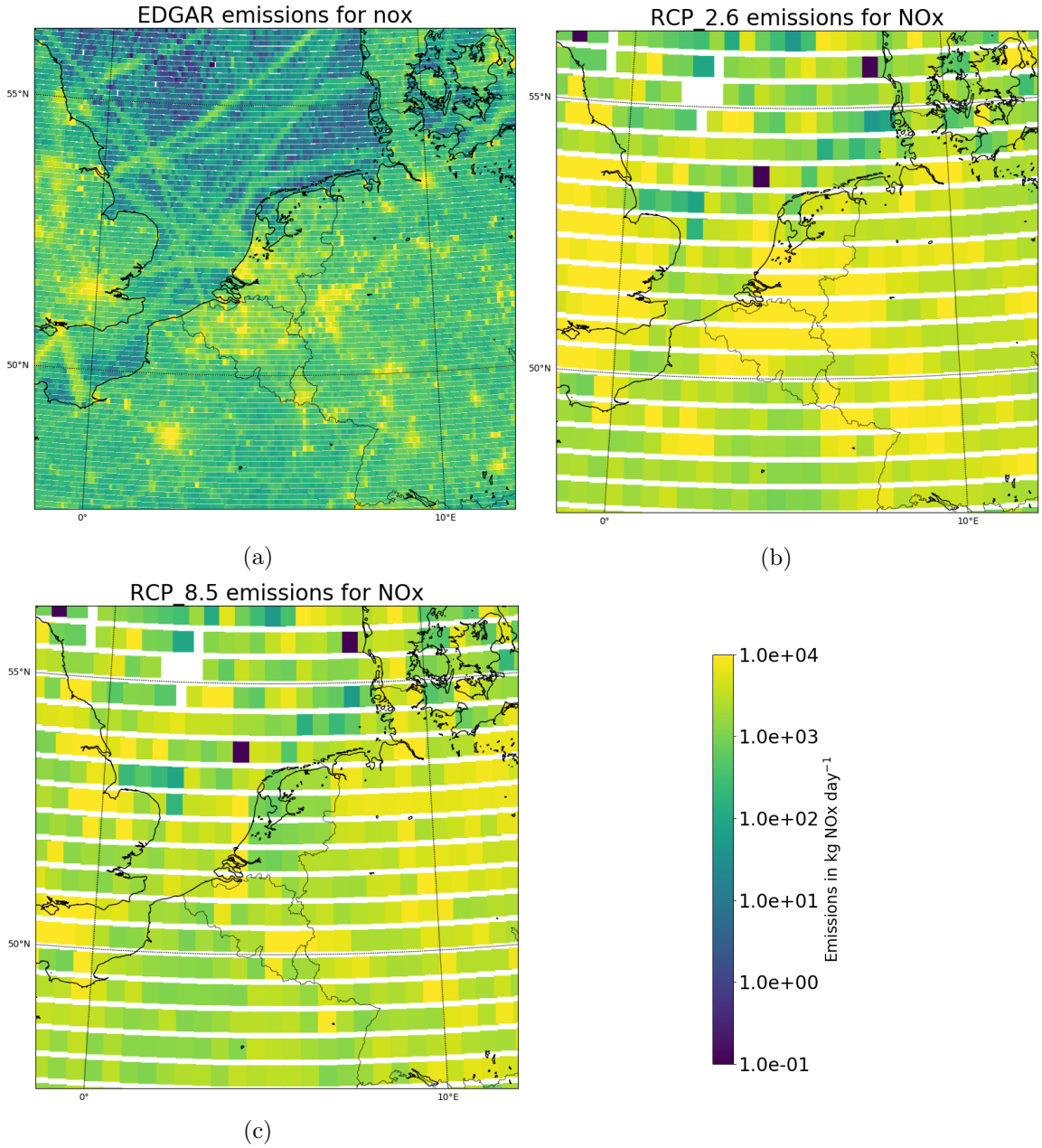

(a) (b)

(c)

Figure 7: NO_x emissions for the different scenarios. (a) is from the EDGAR database for the year 2010, (b) for RCP scenario 2.6 in the year 2050 and (c) for RCP scenario 8.5 in 2050.

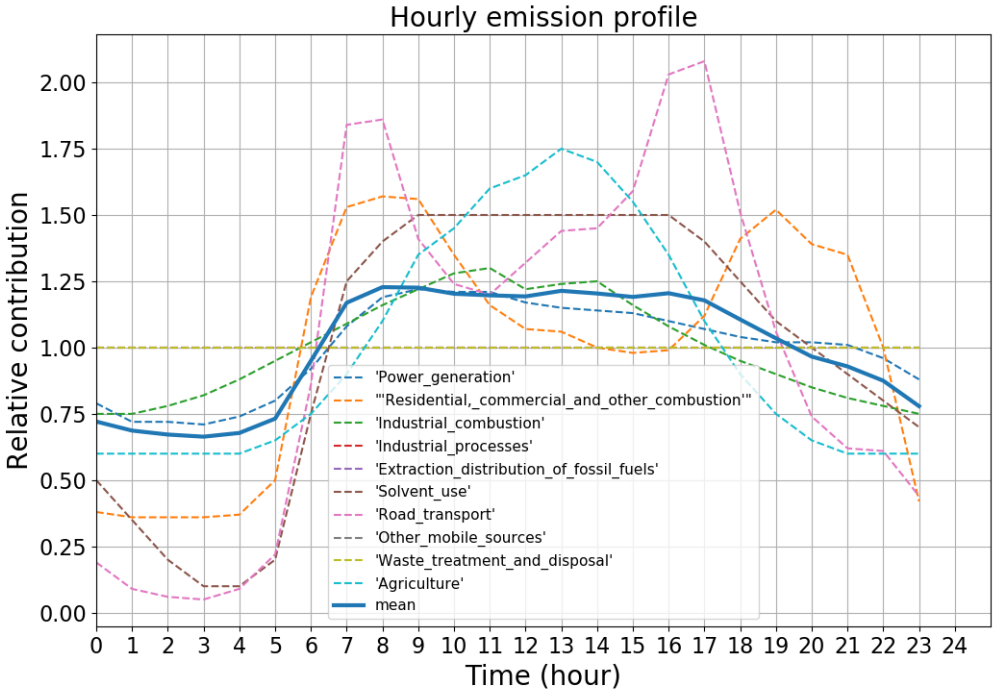

Figure 8: Relative emission intensities of Standardised Nomenclature for Air Pollutants (SNAP) categories every hour for a single day. The mean of all these categories was used to scale the hourly emissions input accordingly.

considered - meteorological forcing and Greenhouse Gas (GHG) forcing.
Meteorological forcing variables that can be prescribed within the model are SST, skin temperature and soil temperature, all of which are taken from model runs of NCAR's Community Climate System Model 4 (CCSM4) (as used in the IPCC AR5 WG1 report) (Gent et al., 2011). These are set as initial conditions as the model calculates its own meteorology for the rest of the run.

	Species	**Concentration** (ppm)	**Reference**
2010	CO_2	389.90	Dlugokencky and Tans, NOAA/ESRL
	CH_4	1798.64 (ppb)	Dlugokencky, NOAA/ESRL
	N_2O	322.50	Dutton et al., NOAA/ESRL
2050 (RCP 2.6)	CO_2	442.70	van Vuuren et al., 2007
	CH_4	1451.54 (ppb)	
	N_2O	341.90	
2050 (RCP 8.5)	CO_2	540.54	Riahi et al., 2007
	CH_4	2734.98 (ppb)	
	N_2O	367.22	

Table 4: Greenhouse gas concentrations used to force the various model runs.

GHG forcing is set within the long wave (RRTM - see table 2) scheme via fixing concentrations of three greenhouse gases (CO_2, CH_4 and N_2O). For the baseline 2010 scenario, mean GHG concentrations were used as measured by NOAA/ESRL, and concentrations for the 2050 scenarios were used as given in the RCP database. Values are given in table 4.

Input data for SSTs for the RCP scenarios are coarser than data for contemporary sce-

narios, which presents some problems in making ozone projections. SST input for future scenarios is particularly coarse, which in a smaller domain with a lot of coastline can be problematic for separations of sea and land. The effect of this is shown in figure 9 - 9a shows the input for 8.5 runs with forcing and 9b the resulting temperature output at 2 metre height for this scenario. There is a clear increase in temperature between land and sea surface, which results in a (potentially unrealistic) ozone build-up over the sea surface. This build up of ozone can then be blown onto land to elevate land-surface ozone concentrations. This is discussed further in section 4.2.3.

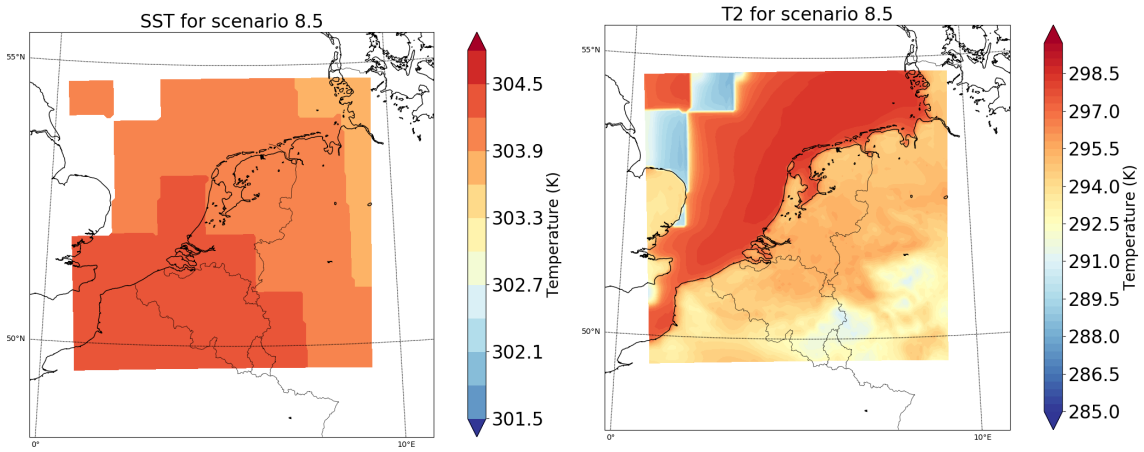

(a) (b)

Figure 9: Sea Surface Temperature (a) and 2m temperature (b) for RCP scenario 8.5.

As a result of this resolution issue, the choice has been made to exclude the area of the domain covered by sea from the end results.

In addition, there is a discrepancy between datasets used to force the baseline and future scenarios - the Sea Surface Temperature dataset from RCP scenarios is between 8 - 15 degrees higher for the summer 2010 period than observational values used to force the baseline runs for the same period. This is the reason for the large temperature increases in the future scenario runs (see figures 20e and 20f) and although this was unintentional, for the purposes of this study a larger temperature increase may give a better indication of ozone-temperature sensitivity.

2.7 Model runs

In order to investigate the effect of climate on ozone but also to separately consider the effects of meteorology and chemistry, multiple runs are needed (eight in total). Two runs in the 2010 period are required - one 'free' run to provide a comparable baseline for the future scenarios and one constrained by meteorological data to compare to observations, and assess if the model is fit for purpose. For the two RCP scenarios, three runs each will be performed: one with updated emissions only, one with updated forcing only, and one full run for the scenario. For consistency, the meteorological/chemical initial and chemical boundary conditions remain unchanged across all model runs. An overview is shown in table 5.

	Input			
Run year	Emissions	Forcing	Meteorology	Run ID
2010 (10-day test)	EDGAR	CFSR SSTs & NOAA GHG concentrations	GFS	Test
2010	EDGAR	CFSR SSTs & NOAA GHG concentrations	GFS	Control
	EDGAR	CFSR SSTs & NOAA GHG concentrations	Free	Free
2050 (RCP 2.6)	EDGAR	RCP 2.6 SSTs/GHG concentrations	Free	2.6_forc
	RCP 2.6	CFSR SSTs & NOAA GHG concentrations	Free	2.6_emis
	RCP 2.6	RCP 2.6 SSTs/GHG concentrations	Free	2.6
2050 (RCP 8.5)	EDGAR	RCP 8.5 SSTs/GHG concentrations	Free	8.5_forc
	RCP 8.5	CFSR SSTs & NOAA GHG concentrations	Free	8.5_emis
	RCP 8.5	RCP 8.5 SSTs/GHG concentrations	Free	8.5

Table 5: Table of runs performed in this study, totaling nine runs for different scenarios.

3 Model Evaluation

In order to use WRF-Chem with confidence to make air quality projections, it is necessary to show that it satisfies model quality requirements for the baseline scenario. A statistical analysis of the model was done for the control run, comparing ozone output to the AirBase network of measurement stations. The AirBase station data is kindly provided by Patrick van Hooydonk (RIVM).

3.1 Statistical tools

The Forum for AIR quality MODelling in Europe (FAIRMODE) has published documentation with guidance on model quality objectives and benchmarking (Janssen et al., 2017), and these guidelines are used when analysing the quality of the model in the prediction of ozone and nitrogen dioxide concentrations. Other, more conventional analysis techniques are used in the comparison of meteorological variables. M denotes model output values and O observational/reanalysis data points.

Mean Bias

$$\text{BIAS} = \frac{1}{N}\sum_{n=1}^{N}(M_n - O_n) = \bar{M} - \bar{O} \tag{3.1}$$

Here, n represents any datapoint in a timeseries at a single location.

Root Mean Squared Error (RMSE)

$$\text{RMSE} = \sqrt{\frac{1}{N}\sum_{n=1}^{N}(M_n - O_n)} \tag{3.2}$$

As measurement errors were not given in the dataset provided, the 95^{th} percentile error (i.e. 95% condfidence interval) is used instead, and is derived in Thunis et al., 2013. Thunis uses hourly ozone measurements from AirBase data as a basis for his derivation, so it is appropriate to use in this study as the same data is being used. The derivation is as follows:

1. Assume u_r^{LV} is a representative relative uncertainty around the Limit Value (LV) for ozone, which is 120 μg m^{-3}. It is fixed to the target uncertainty given in the EU's Air Quality Directive (AQD, 2008).

2. The combined uncertainty on any given datapoint x_n can be decomposed into a proportional component and a non-proportional component with respect to concentration, i.e.
$$u_c^2(O_n) = u_p^2(O_n) + u_{np}^2(O_n)$$

3. The non-proportional component of the uncertainty is by definition independent of the concentration and can be estimated around the LV. It can therefore be defined as a percentage of the LV and assumed to remain constant for all other concentrations
$$u_{np}(O_n) = \alpha\left(u_r^{LV} \cdot LV\right)$$
where α is the non-proportional fraction of the uncertainty around the limit value, between 0 and 1. For ozone, FAIRMODE gives the value to be $\alpha = 0.79$.

4. The proportional fraction of the error can therefore be given in terms of α and the representative relative uncertainty around the LV. This component of the uncertainty is proportional to the concentration, so the LV in the last term will be replaces by the concentration at n
$$u_p(O_n) = (1-\alpha)\left(u_r^{LV} \cdot O_n\right)$$
and the combined measurement uncertainty can then be written as
$$u_c^2(O_n) = (u_r^{LV})^2\left(\alpha^2 LV^2 + (1-\alpha)^2 O_n^2\right)$$

5. From here, an 'expanded uncertainty' is defined. This is done by using a 'coverage factor' k, which is chosen such that the expanded uncertainty represents a 95% confidence interval. In Thunis et al., 2013, this is given as $k_{95} = 2$.
$$U_{95}(O_n) = k_{95} \cdot u_c(O_n)$$
This is known as the 95^{th} percentile measurement uncertainty.

95^{th} Percentile Measurement Uncertainty

$$\mathrm{U}_{95}(O_n) = \mathrm{U}_{95,r}^{LV}\sqrt{(1-\alpha^2)O_n^2 + \alpha^2 LV^2} \tag{3.3}$$

Where $U_{95,r}^{LV} = k_{95} \cdot u_r^{LV}$ is the 95^{th} percentile reference error at the LV, given in FAIRMODE documentation as 0.18 for ozone.
Using the 95^{th} percentile uncertainty, it is possible to calculate the root-mean squared uncertainty for the AirBase observations.

Root Mean Squared Uncertainty (RMS_U)

$$\mathrm{RMS}_U = \sqrt{\frac{1}{N}\left(U_{95}(O_n)\right)^2} \tag{3.4}$$

Correlation Root Mean Squared Error (CRMSE)

$$\mathrm{CRMSE} = \sqrt{\frac{1}{N}\sum_{n=1}^{N}\left(\left(M_n - \bar{M}\right)\left(O_n - \bar{O}\right)\right)} \tag{3.5a}$$

$$\mathrm{CRMSE}^2 = \sigma_O^2 + \sigma_M^2 - 2\sigma_O\sigma_M R \tag{3.5b}$$

Where σ is the standard deviation and R the correlation coefficient. CRMSE is a useful quantity for a deeper analysis of the model performance as it can indicate dominance of certain components of the error, and is related to the RMSE & bias as follows:

$$\mathrm{RMSE}^2 = \mathrm{BIAS}^2 + \mathrm{CRMSE}^2 \tag{3.6}$$

3.2 Model Quality Indicator

The Model Quality Indicator (MQI) is defined by FAIRMODE as the ratio between model bias and a quantity proportional to the measurement uncertainty.

$$\mathrm{MQI}_n = \frac{|M_n - O_n|}{\beta \mathrm{RMS}_U} \tag{3.7}$$

Where n again is a temporal index. β is a coefficient of proportionality which can be set to any value ≥ 1 depending upon how stringent the requirements on the model are. For this study, β is kept the same as in FAIRMODE documentation and is set to 2 (i.e. the

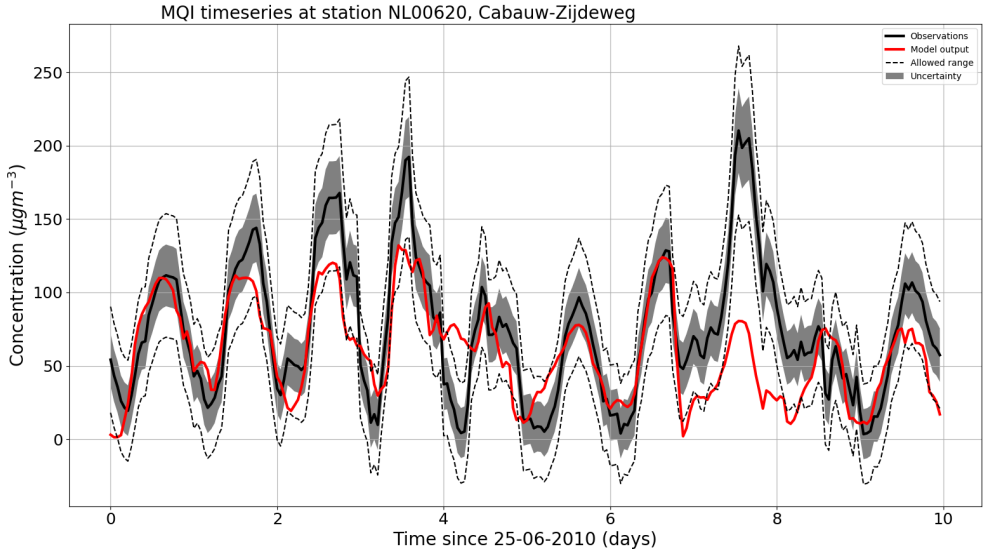

Figure 10: Ozone time series at Cabauw, NL, used for the model evaluation. In red is the model output, black the data from the station, shaded grey the 95^{th} percentile uncertainty and the dotted lines indicate the allowed range, βRMS_U, for the model in order to fulfill the Model Quality Objective.

model output is allowed to be twice the 95^{th} percentile error and would still be considered to be acceptable).
The model output can therefore be evaluated at all locations with available data in this way, and an example is shown in figure 10. A period starting at midnight 25^{th} June and ending at 23:00 on July 4^{th} at the Cabauw tower in the Netherlands is chosen, and plotted in red is the model output at the closest grid point to this station. MQI_n is ≤ 1 at any given time n if the red model output line remains within the dotted lines. This is the definition of the Model Quality Objective.

3.3 Model Quality Objective

The MQI for a given data point n will be ≤ 1 if the model output remains within the dotted lines in figure 10 (i.e. if $|M_n - O_n| \leq \beta RMS_U$), and the Model Quality Objective (MQO) is fulfilled if this is the case. FAIRMODE guidelines stipulate that the MQO must be fulfilled for at least 90% of the available stations. Practically implemented, this means that the MQI at the 90^{th} percentile (after sorting the MQI for every station in ascending order) must be less than or equal to 1.
In order to calculate this, the MQI for every station at each time interval was calculated and ranked in order. The 90^{th} percentile MQI was then extracted for each step, and the average was calculated across all times. If stations had more than 10% of data points missing, these locations were excluded from the analysis.

Model Quality Objective

$$MQO : MQI_{90} \leq 1 \tag{3.8}$$

The results of this analysis are shown in figure 11. Plotted on the y-axis is bias and on the x-axis is CRMSE, both normalised by the uncertainty β RMS_U. Any given station can be plotted on the left or right side of the plot, depending on which error component within the CRMSE dominates, either the correlation coefficient or the standard deviation

(i.e. which term in equation (3.5b) is larger). It is clear that for almost all stations the correlation error dominates, which is not so surprising when considering the variability of a species such as ozone. What is also clear is that WRF-Chem under-predicts ozone at almost every station. Further results will be discussed in more detail in 3.4.

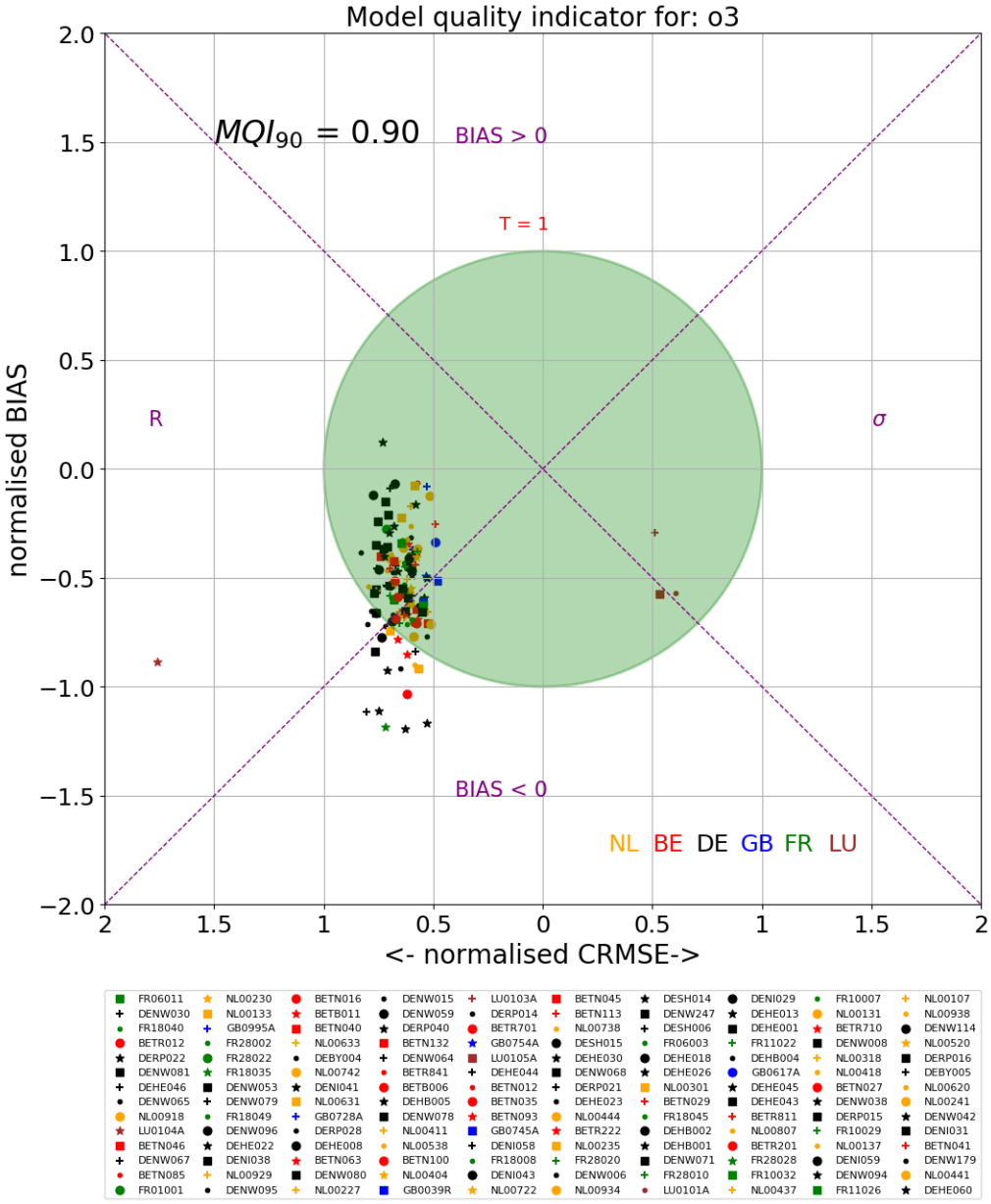

Figure 11: Target diagram for the 10-day WRF-Chem test run using fixed 8-hour averaged ozone data (i.e. 8-hour mean from midight to 8am, then from 8am to 4pm, then 4pm to midnight). The green target area indicates fulfillment of the MQO. In purple, segments are distinguished which indicate whether model error at the station is dominated by bias (positive or negative), standard deviation or correlation. Every individual station is plotted and colour-coded according to the country it is located in. The mean 90^{th} percentile MQI is also indicated in the top left of the plot. Data from 156 stations was used, and the MQI_{90} value indicates that 90% or more of the locations fulfill the MQO criteria.

This MQI is a general performance indicator - overall, the MQO is fulfilled. It is informative, however, to use the CRMSE to investigate the individual error components further for confirmation of the hypothesis that it is the peak values that are missed. By combining

equations (3.5b), (3.6) and (3.7):

$$\mathrm{MQI}^2 = \frac{\mathrm{RMSE}^2}{(\beta\mathrm{RMS}_U)^2} = \frac{\mathrm{BIAS}^2}{(\beta\mathrm{RMS}_U)^2} + \frac{(\sigma_M - \sigma_O)^2}{(\beta\mathrm{RMS}_U)^2} + \frac{2\sigma_M\sigma_O\,(1-R)}{(\beta\mathrm{RMS}_U)^2} \tag{3.9}$$

where R indicates the correlation coefficient. We can examine more closely each of the three Model Performance Indicator (MPI) terms on the right hand side and determine where the error lies. Assuming ideal cases for two of the three Model Performance Indicator allows formulation of the Model Performance Criteria (MPC), conditions which are necessary but not sufficient for fulfillment of the MQO. As an example, assuming that the model output correlates perfectly with observations (R = 1) and the standard deviations are equal ($\sigma_M = \sigma_O$) leads us to an expression for the MPI for BIAS:

$$\mathrm{MQI} = \frac{\mathrm{BIAS}}{\beta\mathrm{RMS}_U} \qquad \text{and} \qquad \mathrm{MPC:}\ \frac{\mathrm{BIAS}}{\beta\mathrm{RMS}_U} \leq 1$$

This approach can also be applied to the other two terms. The MPI and MPC generated are listed in table 6.

MPI	**MPC**	**Percentage of stations fulfilling MPC**
BIAS (R = 1, $\sigma_M = \sigma_O$)	$\lvert\mathrm{BIAS}\rvert \leq \beta\mathrm{RMS}_U$ (3.10)	94.7%
R (BIAS = 0, $\sigma_M = \sigma_O$)	$\mathrm{R} \geq 1 - \beta^2 \frac{\mathrm{RMS}_U}{2\sigma_M\sigma_O}$ (3.11)	71.2%
SD (BIAS = 0, R = 1)	$\lvert\sigma_M - \sigma_O\rvert \leq \beta\mathrm{RMS}_U$ (3.12)	97.4%

Table 6: Necessary but not sufficient criterion for the MQO to be fulfilled. The third column indicates how many stations in the domain fulfill the MPC.

3.4 Quality Analysis

As is indicated by figure 11, at stations where the quality criteria is not met, this tends to be because of underestimation (and to a limited extent on correlation). On almost every station the bias is negative. This is somewhat to be expected of any ozone models, as high ozone events can be difficult to predict. If an ozone 'event' is defined as any time where the maximum daily 8-hour averaged ozone rises above 120 μg m^{-3}, then on average WRF-Chem fails to predict 5 events over a 10-day test period (i.e. 30 possible events). Further towards the coast the model performs reasonably well, although events here are also much less common in the data (i.e. ozone is generally lower and events occur much less frequently). Further inland and especially in the area south of the Ruhr region in Germany the model performs relatively poorly with regard to these events. Measured

ozone here is very high, with some night-time concentrations remaining above the 120 μg m^{-3} limit. Heavy industrialisation in this region has a lot of influence on daily ozone peaks and fluctuations in activity are difficult to parameterise within emissions databases. It seems likely therefore that, at least southeastern corner of the domain, underprediction is the result of discrepancies between actual and parameterised emissions. The variability of ozone is captured well though, as indicated by the fact that a high percentage of stations fulfill the quality criterion for standard deviation.

4 Results

In this section results from all runs will be presented, beginning with the contemporary scenarios and ending with future ones.

4.1 Baseline (2010)

To make useful comparisons about ozone changes with regard to climate a baseline scenario has to be established. The 'free' run (see table 5) will be used as a baseline for comparison directly with future scenarios, and the constrained run will serve as a reference for the 'free' run.

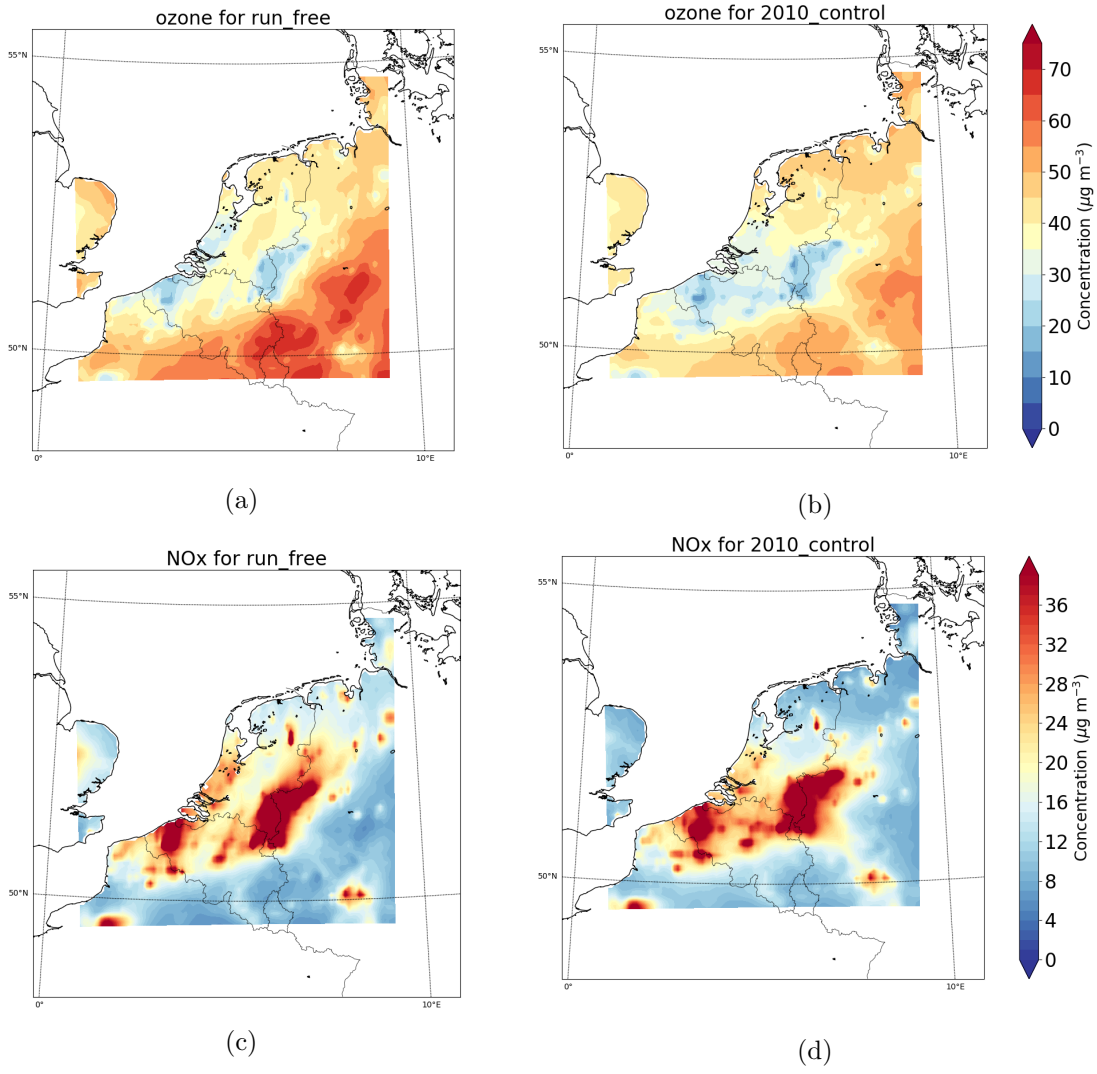

Figure 12: Time-averaged hourly ozone and NO_x concentrations for meteorologically constrained and free runs. Figures (a) and (b) show ozone concentrations for the free and constrained scenario respectively, (c) and (d) the same for NO_x.

The 2 metre mean temperature of the free run is generally lower than that with constrained meteorology, by about 2-3K and as much as 6K in some places. This does not appear to influence the ozone concentrations much, and the effect from NO_x concentration differences dominates, as shown in figure 12. The spatial distribution of ozone in both runs is similar. Higher mean concentrations are found further inland, across the southeastern corner of the domain, and both scenarios display an ozone suppression along the southern half of the

Dutch-German border and the Belgian coastline. This is mirrored in the NO_x distribution - where ozone is suppressed NO_x is elevated. NO_x concentrations are largely dependent on emissions and only to a limited extent on meteorology (evidenced by similarity in NO_x distribution to locations if high emissions in figure 7a), so as the same emissions dataset is used in both runs (and despite the temperature disparity) the NO_x concentration distribution is also very similar.
In general, ozone levels are slightly lower in the control scenario than in the free run, and vice versa for NO_x levels. This can be explained largely through a difference in calculated cloud cover in the two runs - the control scenario has more cloud cover, especially around coastal regions and around the points of higher NO_x. In addition, the wind in the free run around coastal regions blows more parallel to the coast rather than perpendicular, as is the case in the control run, meaning that less 'clean' air from the ocean is blown in across the land and more pollution is brought in from continental Europe.

4.2 2050 scenarios

To answer the research questions posed at the start of this thesis, we consider the average ozone level over the whole June-July August period, while also counting the number of ozone spikes (8-hour mean concentrations >70 μg m^{-3}) which are more dangerous to human health. First the change in ozone due to changes in emissions and forcing will be evaluated, and thereafter the health impact will be quantified.

4.2.1 Emissions

As can be inferred from figure 12, the domain is in the VOC-limited regime (i.e. where there is more NO_x there is less ozone, and vice versa). This means that if emissions of NO_x increase, then ozone should decrease. Figure 7 shows that RCP scenario 2.6 has the highest emissions for the domain in the year 2050, so we expect that this scenario will have the lowest ozone and lowest Relative Risk accordingly. The temperature differences as a result of differing emissions are marginal (on the order of 0.1 K) so ozone differences as a result of temperature changes, either direct or via NO_x concentrations, are likely to be negligible.

Figure 13 shows that a change in emissions of NO_x has a clear effect on ozone. Where NO_x increases ozone decreases, and vice versa, in both scenarios. For NW Europe the emissions-only run for RCP 8.5 exhibits a strong NO_x decrease (>30 μg m^{-3}) in border regions, a patch in the Frankfurt region and along the Belgian coast, resulting in mean ozone concentration increases of more than 30 μg m^{-3} in these areas. In the rest of the domain there is relatively little change in NO_x concentration (between -5 to 5 μg m^{-3}) which is reflected in more modest changes in ozone concentrations (although transport of ozone from peak regions keeps the change positive).

The emissions-only run for RCP 2.6 also exhibits sharp NO_x decrease of similar magnitude in the same regions as in the RCP 8.5 emissions run - however, the effect is limited to a much smaller area within these regions, and is possibly the result of resolution differences between 2010 and 2050 datasets. Most of the locations where NO_x decreases correspond to areas of higher NO_x emissions in 2010 (figure 7a). In a higher resolution dataset the emissions are concentrated into a smaller area and therefore are higher in those areas. The lower resolution spreads these emissions over a larger area and may represent a similar overall amount of NO_x emitted, but distributed differently. Generally though, the domain shows a widespread increase in NO_x of between 5-10 μg m^{-3}. Ozone in response decreases by between 5 and 15 μg m^{-3}.

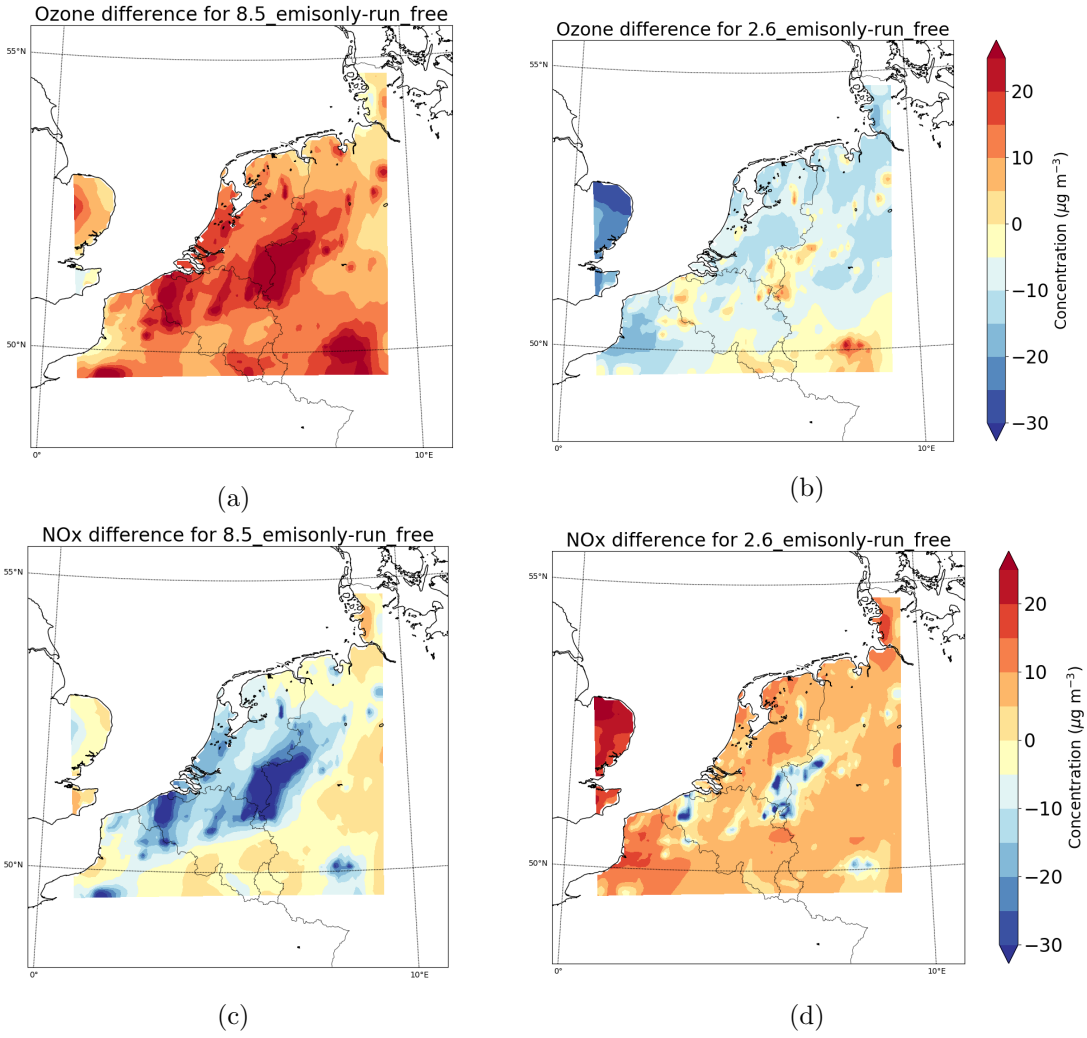

Figure 13: Difference in the time-averaged concentration across the summer periods of 2010 and 2050 of hourly ozone and NO_x concentrations for the emission-only runs for RCP scenarios 8.5 and 2.6, as compared with the free baseline scenario. Figures (a) and (b) show the ozone concentration change, and (c) and (d) the NO_x change for RCP 8.5 and 2.6, respectively.

4.2.2 Forcing

Climatic change (i.e. difference in wind direction/speed & temperature, amongst others) for the forcing-only run for RCP 2.6 is limited, and so too are any changes in ozone or NO_x levels. There is a significant temperature increase in the forcing-only run for RCP 8.5, with an associated increase in short-wave radiation.

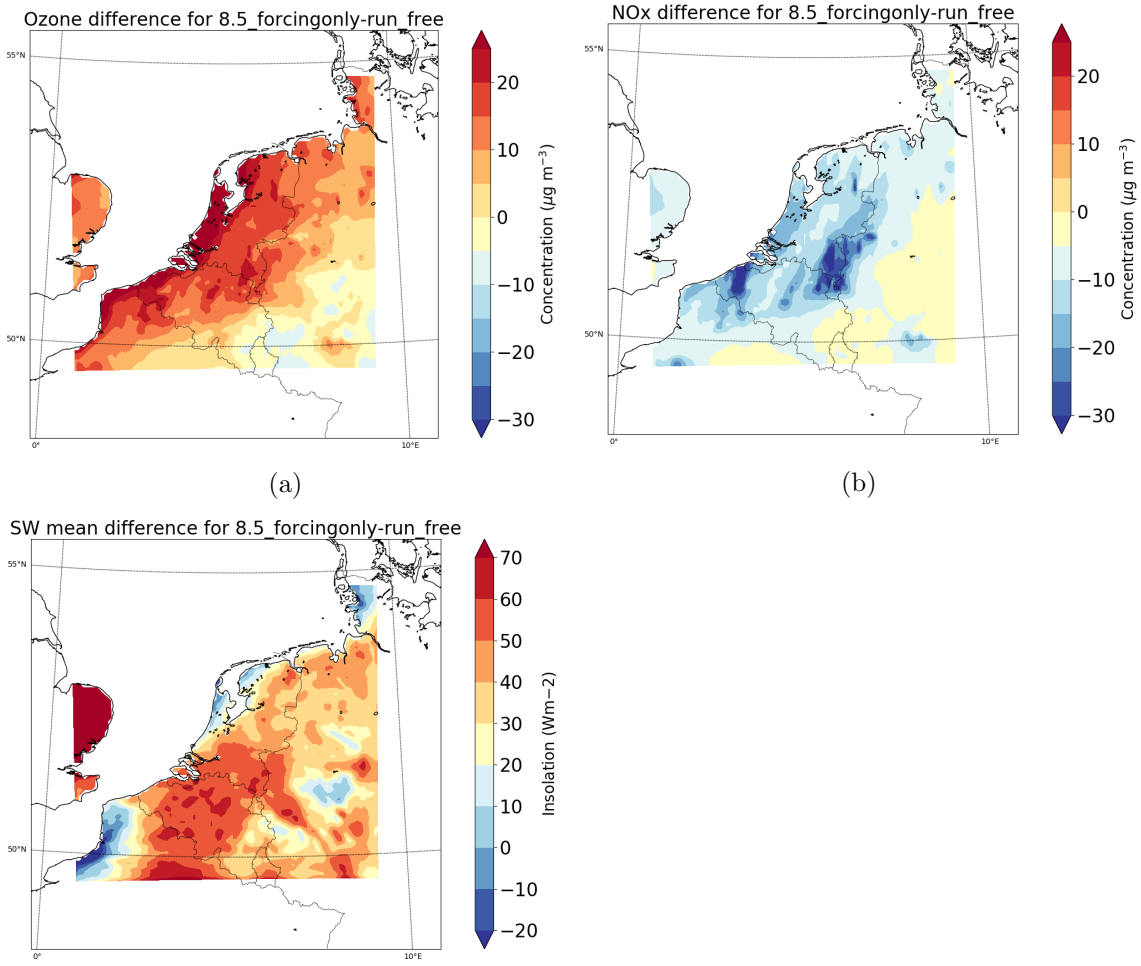

Figure 14: Time-averaged changes for run 8.5_forcing in ozone (a) and NO_x (b). (c) shows the difference in cumulative short-wave radiation received by the surface over the three month period.

The emissions input does not change from the baseline scenario to the forcing-only run for RCP 8.5, so all NO_x concentration changes shown in figure 14b are as a result of meteorological changes. In general higher temperatures (see figure 20e) are indicative of more short-wave radiation (figure 14c) and thus a higher rate of NO_2 photolysis. This however relies on there being enough NO_x present to photolyse, illustrated by the large increase in short-wave radiation on the left side of the southern edge of the domain, with no discernible reaction from either ozone or NO_x. This is a good indicator that ozone is indirectly influenced by temperature via NO_x. Nonetheless, direct correlation between ozone and 2 metre temperature does increase between the baseline scenario and the RCP 8.5 forcing run (from 0.46 to 0.66), although still remains weaker than the ozone-NO_x correlation. Figures 15 & 16 support this assessment - correlations between ozone and NO_x concentrations are highest regardless of the forcing/emission combination or RCP

scenario. Ozone-temperature correlations follow NO_x-temperature correlations: when the NO_x-temperature correlation is strong then so is that of ozone-temperature, and vice versa. Ozone-temperature correlations are strongest in the forcing runs of both scenarios, as are NO_x-temperature correlations.

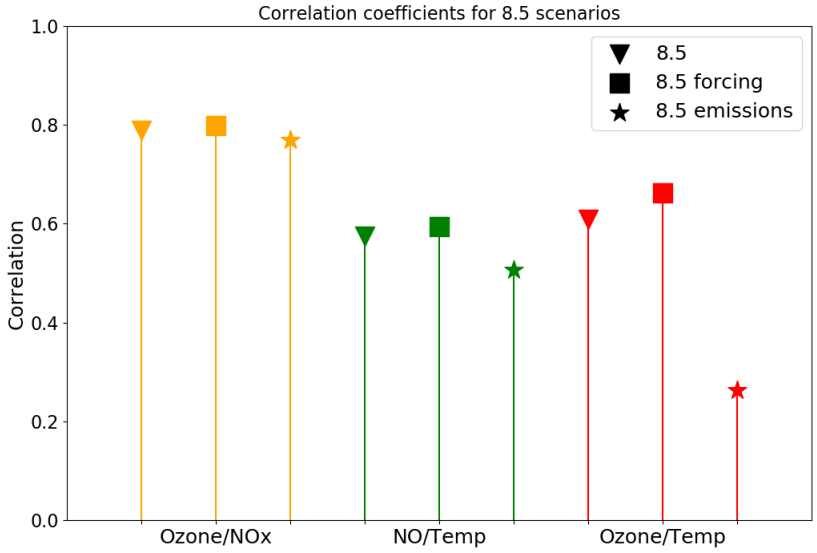

Figure 15: Correlations (absolute value) between Ozone, 2m temperature and NO_x for scenario 8.5 runs. Ozone/NO_x and NO_x/temp correlations are negative.

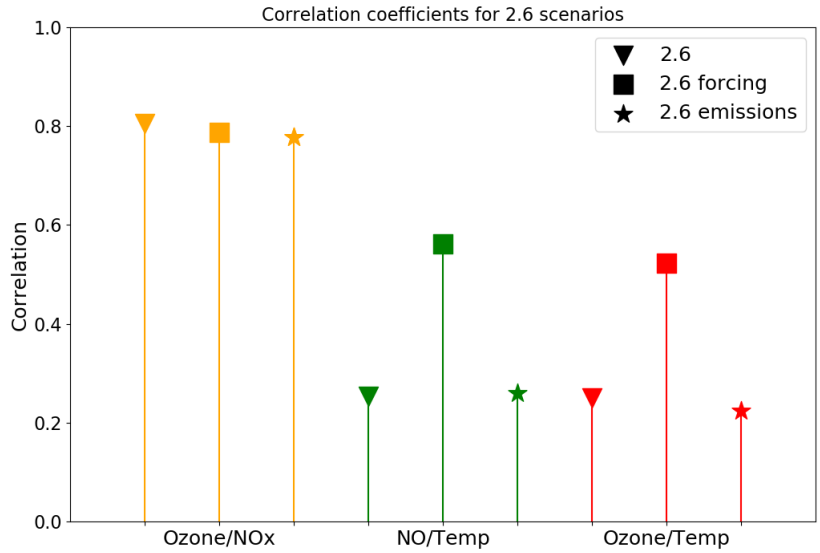

Figure 16: Correlations (absolute value) between Ozone, 2m temperature and NO_x for scenario 2.6 runs. Ozone/NO_x and NO_x/temp correlations are negative.

The magnitude of ozone concentration differences in the RCP forcing scenario 8.5 is similar to that in the emissions run. However, spatial distribution is very different between the two scenarios. The main areas of decrease in NO_x in both scenarios remain in similar locations but in the RCP 8.5 forcing scenario NO_x decrease is spread somewhat further from the more significantly reduced regions. The ozone increase is correspondingly more spread in the forcing scenario, but the pattern changes to one decreasing further from the coast. Reasons for this will be examined in the following section.

4.2.3 Full RCP scenario

In the run for RCP 2.6, the change in temperature is minimal (mean difference across the whole domain is 0.2 K) so both figures 13b and 20b are very similar - clearly controlled by chemical processes much more than meteorological ones. The situation for the run for RCP 8.5 is different, although further away from the coastline figures 13a & 20a still bear remarkable similarities in profile despite a large (on average +10.9 K) temperature difference (the large temperature difference due to dataset discrepancies, as discussed in section 2.6). This means the future scenario is not accurately represented, but this is not an issue when considering the sensitivity of ozone concentrations to climate change. Temperature rise is reduced further inland (figure 20e) but still remains around the +5 K level across the more southern part of Germany in the domain. Despite this, ozone increase is limited to 5-10 μg m^{-3} in this region, in line with an NO_x decrease of between 0 and 10 μg m^{-3}. The increase along the coastline is in part due to the NO_x decrease observed along the Belgian coast but particularly along the Dutch coastline North Sea ozone is blown by the prevailing wind (south-westerly) landwards. In general NO_x emissions are lower over the North Sea (except along ship trails) and dry deposition of ozone does not occur, so concentrations can build up to higher levels than over land. Once ozone is blown onto land it can deposit and concentrations quickly reduce, but the wind direction (figure 17) is such that ozone is blown into the Netherlands and the northerly tip of France, and spikes (8-hourly mean concentrations >70 μg m^{-3}) occur more frequently in these areas.
The magnitude of the changes in ozone concentration is for the most part in line with previous studies done (Weaver et al., 2009) (see section 0), despite the large temperature increase. This suggests that something other than temperature/forcing is directly controlling ozone levels.

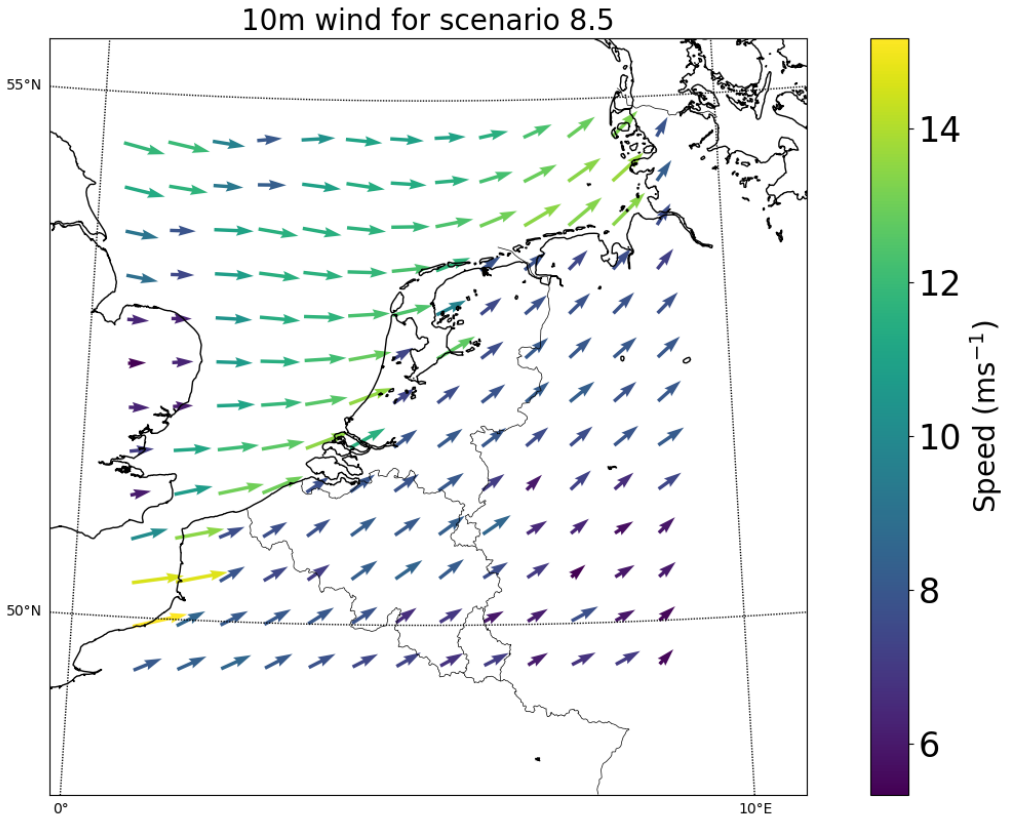

Figure 17: Wind speed and direction for RCP scenario 8.5.

It is apparent that though the temperature increase is significant in all parts of the domain (+4 degrees or more) the mean ozone concentration is not so sensitive to this, but rather more to NO_x concentrations. Especially when considering ozone spikes, if the lowest recorded NO_x concentration for a given day is above around 6-8 μg m^{-3}, the chances of an ozone spike occurring are small. This is illustrated in figure 18. 74 % of all ozone spikes occur if NO_x concentration dips below 2 μg m^{-3} in the course of the day, and over 97% of spikes occur on days where the concentration dips below 4 μg m^{-3}.

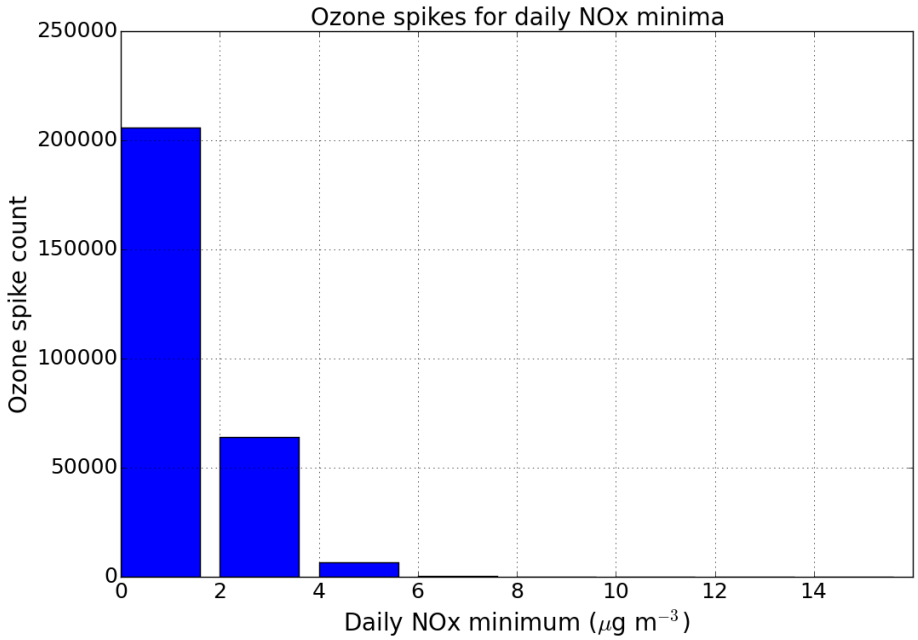

Figure 18: A graph showing the number of ozone spikes (8-hourly mean concentrations >70 μg m^{-3}) for given intervals of daily NO_x minima, across all data points for scenario 8.5.

There is a pattern with temperature too, and over 70% of ozone spikes occur when the daily maximum temperature is above 300 K (27^{o}C). Nonetheless there remains a chance of a spike occurring at lower temperatures (figure 19), and the arresting effect of higher NO_x concentration causes a much sharper drop in spikes in the RCP 8.5 run than higher temperatures does in increasing spikes. This further supports the idea of NO_x as the limiting factor in peak ozone concentrations.

4.3 Health Impacts

The baseline for adverse health effects (set at 8-hour mean concentrations of 70 μg m^{-3}) is regularly exceeded in most runs. The Relative Risk was calculated as in section 1.1, and the change with respect to the baseline scenario is shown in figure 21.
Figure 21b shows little change in the Relative Risk (ratio of ozone-related mortality in exposed population to unexposed population) across most of the domain. It remains less than +0.1% except for an increase of around +0.2% (confidence interval 0.1% - 0.4%) along the southern edge of the domain covering Belgium, Luxembourg and Germany, and also a small fraction of coastline in NW Germany. As seen in the baseline scenario (figure 12a) ozone concentrations tend to be higher further inland, thus chances of ozone spikes (>70 μg m^{-3}) are higher here.
For run 8.5 the ozone spikes occur with more frequency and spread over the whole domain and so the Relative Risk increase is kept around +0.25% (>0% and <0.4%) for the

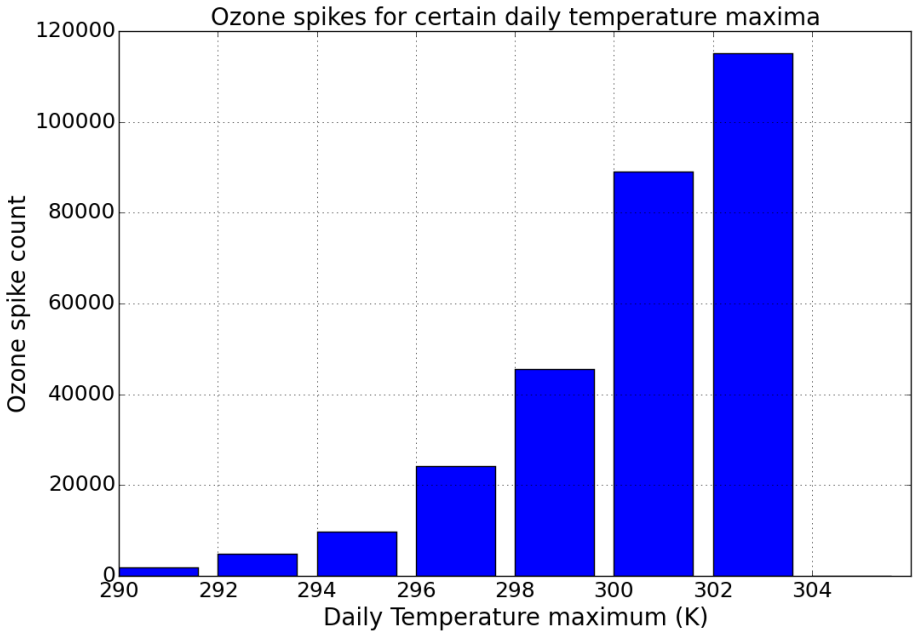

Figure 19: A graph showing the number of ozone spikes (8-hourly mean concentrations >70 μg m^{-3}) for given intervals of daily temperature maxima, across all data points for scenario 8.5.

majority of grid points. The Dutch coastline shows a significant increase of +0.4% (0.2% to 0.6%), in line with larger ozone increases and more frequent spikes in the area. In the southwestern corner of the domain there is also a marginally higher level of risk (+0.3%) but with a larger confidence interval range (>0% and <0.6%). A reasonable number of spikes were recorded here (figure 21c), so the larger confidence interval indicates that in the number that did occur there, not many were significantly greater than daily 8-hour mean concentrations of 70 μg m^{-3}.
To put this all into context, and average increase in RR of 0.25% across the summer period in the Netherlands results in a 17-18% increase in the number of deaths attributable to ozone over the same period, and a maximum average risk increase of 0.6% causes up to a 54% increase for the three summer months. As an example, currently between 200-300 people in the Netherlands die each year as a result of ozone pollution. If 1/4 of these deaths occur in the summer months (and likely this fraction is larger) then, off the basis of the increase in risk calculated, between 8-40 additional deaths are projected for June, July and August of 2050 in the Netherlands.

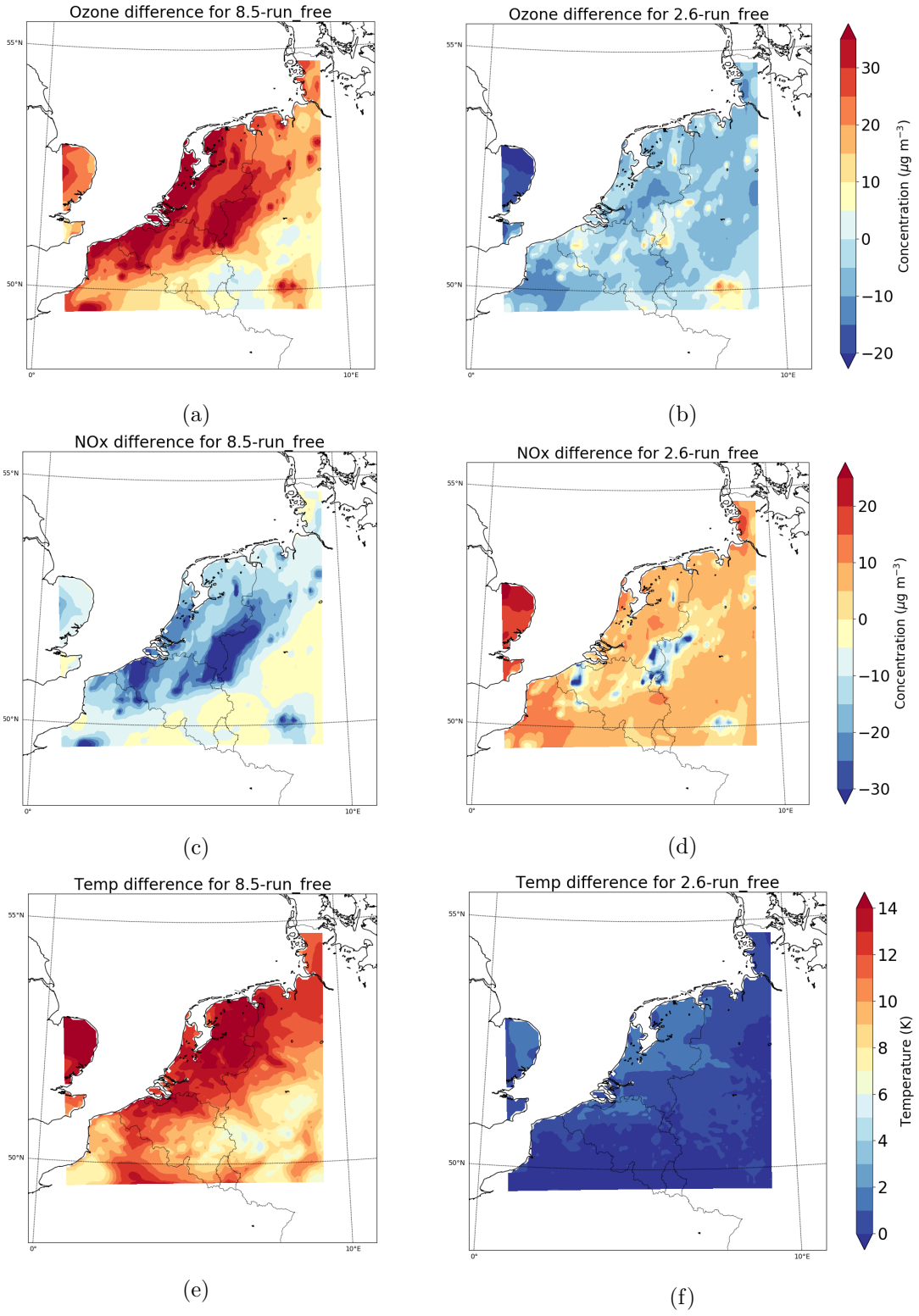

Figure 20: Difference between the time-averaged concentration across the summer 2010 & 2050 periods or hourly ozone (a & b), NO_x (c & d) and 2-metre temperature (e & f) for runs 2.6 (b, d & f) and 8.5 (a, c & e) as compared with the free baseline scenario.

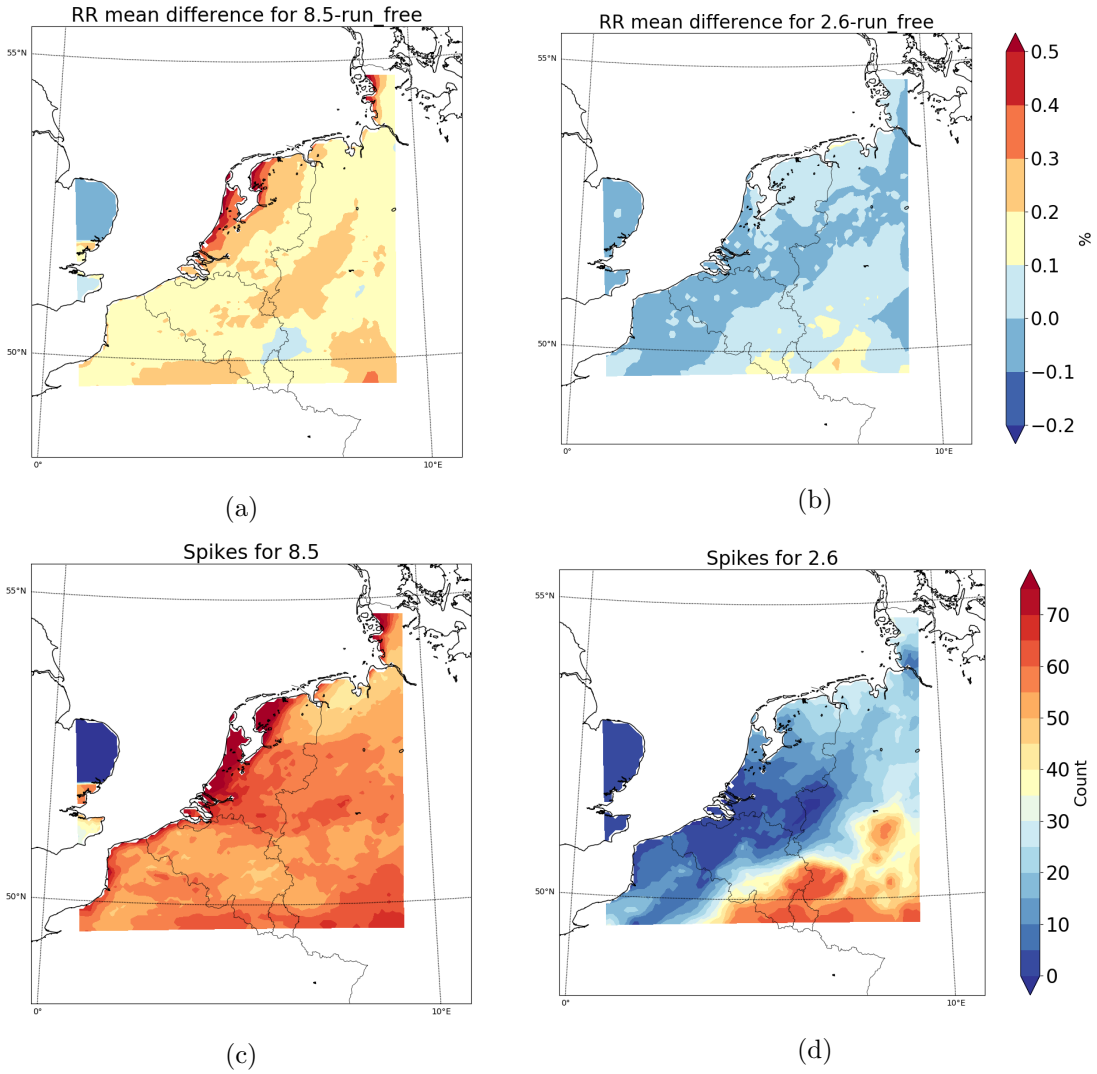

Figure 21: Time-averaged change in Relative Risk (i.e. ratio of ozone-related mortality in exposed population to unexposed population) over the summer period for run 8.5 (a) and 2.6 (b). (c) and (d) show the number of ozone spikes (8-hourly mean concentrations >70 μg m^{-3}) per grid point over the whole run period for 8.5 and 2.6, respectively.

5 Conclusions

In this section the three research questions presented in the introduction will be answered, and methods used in this study will be discussed.
As with any study, there are some caveats that should be taken into account with any conclusions presented in this study.
Firstly, care was taken to use the most up-to-date emission datasets containing full speciation and spatial distribution of all VOCs for both the 2010 and future scenarios. However, ozone in models is sensitive to VOC speciation (von Schneidemesser et al., 2016) so possible differences between EDGAR and RCP emission datasets may result in exaggerated or understate changes in ozone between runs. A further complicating matter is the difference in resolution between the two datasets - a coarser resolution can extend the effects of a polluting city to the surrounding area, for example.
Secondly, it is difficult to assess WRF-Chem's representation of future weather events which may play a role in daily 8-hour mean ozone rising above 70 μg m^{-3}. Future scenarios were based only on forcing from Sea Surface Temperatures & greenhouse gas concentrations, from which the model was allowed to calculate its own meteorology. A period of 3 months is relatively short, so a small number of these weather events (or a lack thereof) can make a significant difference to spike count. Further, larger domain studies such as those examined in Weaver et al. (2009) across the USA show variations in regional patterns of ozone concentrations - regions of a similar size to the central domain modeled in this study - dependent on meteorology.
Third, it must be stressed that the "RCP" scenarios used in this study are not intended to be accurate representations of the scenarios themselves - rather, aspects of the scenarios (emissions and forcings) are used to measure ozone response. The model was effectively spun-up from a 2010 ground state with parts of 2050 climate.
Fourth, tropospheric ozone is a very variable species and modeling it over such a short period of time will always present problems in assessing a general trend. A single summer period may give an indication of which direction trends are in but is simply not enough time to gain reliable insight into the influences changes in out climate may have on future ozone concentrations. Running for longer periods on the resolution used here is currently still too computationally expensive to show diurnal patterns of any meteorological or chemical variable.
Fifth, temperature change for the future scenario, RCP 8.5 in particular, was too large to be realistic. However as mentioned previously, this does not cause a problem for assessing the sensitivity of ozone to climate change.
Sixth and finally, emissions parameterisation is difficult. A daily profile was used for each day, and therefore the model misses ozone changes due to deviations from this profile, a high probability (because of changes in traffic, demands on power plants & industry etc). As ozone appears to be more limited by its chemistry than meteorology, this may prove to be an important factor in model inaccuracies.

How does ozone change with changing climate?

In all scenarios NW Europe remains VOC-limited, so ozone levels in general remain controlled by emissions of NO_x. In a scenario with fewer emissions ozone levels rise, and vice versa. Ozone above the sea is not in this regime however, and so rises significantly with the changes in forcing. This indicates the important limiting role NO_x plays, as in its absence temperature and forcing can result in relatively large concentration increases. The magnitude of these increases is within the range of ozone increases from previous

studies, which given that the temperature increase in this study was significantly larger than other studies further reinforces this point. Correlation between ozone and NO_x is the stronger than ozone/temperature correlation in every future run and does not deviate from around -0.7 to -0.8. There are some differences between full scenario runs and runs with the emission component only across the whole domain, indicating that climate does exert a certain degree of influence, but as NO_x/temperature correlations across model runs follow ozone/temperature correlations closely, it seems more likely that this is an indirect influence via NO_x.

Are ozone spikes more sensitive to anthropogenic emissions or meteorology in a future climate?

WRF-Chem points to NO_x being the limiting factor in ozone spikes. High ozone events occur somewhat less frequently at lower temperatures compared to higher temperatures, but no more than 3% of spikes occur on days when the NO_x concentration rises above 4 μg m^{-3} in the higher temperature scenarios. Indeed, there are some areas in figure 20 where temperature increases result in no discernible change in ozone concentration. Less NO_x is in part result of more insolation so there is some meteorological influence, but the chemistry of the system is somewhat more dominant in limiting the occurrence of spikes.

What is the risk to human health?

In a lower forcing future climate scenario the Relative Risk does not change significantly - for the majority of the domain it remains between -0.1% to +0.1%. In the higher forcing scenario this mean risk is elevated by up to and additional +0.6% in some places. Relative Risk is a daily quantity however, and in some places in scenario 8.5 the risk on a single day rise as high as 2.6% (1.3% to 3.9%), whereas the highest values in the baseline scenario are around 1.2% (0.6% to 1.7%). As previously mentioned WRF-Chem has problems simulating ozone spikes however, and observational data for the summer of 2010 returns RR values as high as 4.1% (2.0% to 6.2%), so any absolute Relative Risk are almost certain to fall far short of actual 2050 (even if there are no major shifts in climate). Nonetheless, with a higher forcing climate scenario risk of mortality associated with ozone is shown to increase, and thus the number of ozone-related deaths to rise by approximately 17-18%.

Limitations in this study preclude the drawing of these conclusions with any certainty, and the author has several suggestions as to how more confidence can be placed in the results presented herein.

- A unification of input data sets would improve accuracy in representing RCP scenarios, and thus perhaps a more accurate projection of future climate. Discrepancies in current and projected climate (both in the data itself and differences in resolution) mean that absolute values cannot be taken at face value. Applying a relative change based on RCP scenario projections to contemporary reanalysis datasets, such as those used for the baseline scenarios, may be an appropriate method to achieve this. Incrementally increasing the 2010 SSTs based on the future forcing scenarios, and similar for emissions, is suggested by the author. Differences in NMVOC speciation between current and future emission parameterisation may also have a significant effect on calculated ozone concentrations.
- Emission parameterisation is still a bottleneck for modeling species such as ozone with chemistry so dependent om emitted species. Ozone spikes are caused at least in

part by fluctuations in emissions from specific areas so to capture every peak is extremely difficult. Emissions data used as input in this study consisted of an average daily profile for the full sumer period, which is unrealistic and does not represent variations in anthropogenic activity (e.g. variations in traffic on the roads, day-to-day changes in industrial activity, higher/lower power consumption & electricity production etc). More accurate emission schemes, perhaps also more regional emission schemes, would be a step towards improving model accuracy with regards to variability and capturing peak values. Further investigation into the potential weightings of different sources of anthropogenic emissions (i.e. Standardised Nomenclature for Air Pollutants (SNAP) categories) may also be warrented.

- Longer runs, with more datapoints and also including other seasons will give a better idea of trends in ozone concentrations. Natural variability and potential existence of several (or none at all) extremes in temperature or weather events may skew results in a single summer period which would be smoothed out by running for a longer time period, or for the same time period for a number of years closer together (e.g all summers over the decade 2045-2055).

Nonetheless, with regional air quality models it has been possible to examine some aspects of the influence climate change may have on the air we breathe, and examine more closely the local changes that may occur as a result of the larger changes we as human beings are bringing about on our planet.

References

[1] AQD. *Directive 2008/50/EC of the European Parliament and of the Council of 21 May 2008 on Ambient Air Quality and Cleaner Air for Europe (No. 152), Official Journal.* European Union, May 2008. https://eur-lex.europa.eu/legal-content/EN/TXT/PDF/?uri=CELEX:32008L0050&from=EN.

[2] J.P. Beck, M. Krzyzanowski, B. Koffi, A.G Hjellbrekke, H. Hootsen, Millán M. Millán, M. Tombrou, and D. Simpson. *Tropospheric Ozone in the European Union "The Consolidated Report"*. European Environment Agency, November 1998.

[3] Megan Bela, Stuart McKeen, Mary Barth, Gabriele Pfister, Christine Wiedinmyer, and Louisa Emmons. *Biogenic, Wildfire, Lightning, and Volcano Emissions in WRF-Chem [Powerpoint slides].* The WRF Users' Basic Tutorial, July 2017. Retrieved from: https://ruc.noaa.gov/wrf/wrf-chem/wrf_tutorial_2017/MEGAN_LTNG_WRFchemTutorial.pdf.

[4] David C. Carslaw. Evidence of an increasing no2/nox emissions ratio from road traffic emissions. *Atmospheric Environment*, 39(26):4793 – 4802, 2005.

[5] M. Crippa, G. Janssens-Maenhout, F. Dentener, D. Guizzardi, K. Sindelarova, M. Muntean, R. VanÂ Dingenen, and C. Granier. Forty years of improvements in european air quality: regional policy-industry interactions with global impacts. *Atmospheric Chemistry and Physics*, 16(6):3825–3841, 2016.

[6] Ed Dlugokencky. Trends in Atmospheric Methane. www.esrl.noaa.gov/gmd/ccgg/trends_ch4/. NOAA/ESRL. Accessed: 2018-04-15.

[7] Ed Dlugokencky and Pieter Tans. Trends in Atmospheric Carbon Dioxide. www.esrl.noaa.gov/gmd/ccgg/trends/. NOAA/ESRL. Accessed: 2018-04-15.

[8] Geoffrey S. Dutton, James W. Elkins, and Bradley D. Hall. Nitrous Oxide data from the NOAA/ESRL halocarbons in situ program. https://www.esrl.noaa.gov/gmd/hats/insitu/cats/conc.php?site=mlo&gas=n2o. NOAA/ESRL. Accessed: 2018-04-15.

[9] EC. *Air Quality Standards.* European Comission, 2017. Accessed 3 May 2018.

[10] EEA. *Ozone and particulates most serious air quality problems in Europe.* European Environment Agency, 2011. https://www.eea.europa.eu/highlights/ozone-and-particulates-most-serious.

[11] EEA. *Exceedance of air quality standards in urban areas.* European Environment Agency, 2017. https://www.eea.europa.eu/data-and-maps/indicators/exceedance-of-air-quality-limit-3/assessment-3.

[12] EMEP. *Transboundary particulate matter, photo-oxidants, acidifying and eutrophying components.* European Monitoring and Evaluation Programme, September 2016. http://www.emep.int/publ/reports/2016/EMEP_Status_Report_1_2016.pdf.

[13] L. K. Emmons, S. Walters, P. G. Hess, J.-F. Lamarque, G. G. Pfister, D. Fillmore, C. Granier, A. Guenther, D. Kinnison, T. Laepple, J. Orlando, X. Tie, G. Tyndall, C. Wiedinmyer, S. L. Baughcum, and S. Kloster. Description and evaluation of the Model for Ozone and Related chemical Tracers, version 4 (MOZART-4). *Geoscientific Model Development*, 3(1):43–67, 2010.

[14] Gidon Eshel and Joseph J. Bernstein. Relationship between large-scale atmospheric states, subsidence, static stability and ground-level ozone in illinois, usa. *Water, Air, & Soil Pollution*, 171(1):111–133, Apr 2006.

[15] Peter R. Gent, Gokhan Danabasoglu, Leo J. Donner, Marika M. Holland, Elizabeth C. Hunke, Steve R. Jayne, David M. Lawrence, Richard B. Neale, Philip J. Rasch, Mariana Vertenstein, Patrick H. Worley, Zong-Liang Yang, and Minghua Zhang. The community climate system model version 4. *Journal of Climate*, 24(19):4973–4991, 2011.

[16] G. A. Grell, S. E. Peckham, R. Schmitz, S. A. McKeen, G. Frost, W. C. Skamarock, and B. Eder. Fully coupled "online" chemistry within the WRF model. *Atmospheric Environment*, 39:6957–6975, 2005.

[17] G. A. Grell and S. R. Freitas. A scale and aerosol aware stochastic convective parameterization for weather and air quality modeling. *Atmospheric Chemistry and Physics*, 14(10):5233–5250, 2014.

[18] G. A. Grell and R. Ahmadov. WRF-Chem V3.8: A summary of status and updates. In *17th WRF users' workshop*. NOAA, Earth System Research Laboratory, June 27 - July 1 2016. http://www2.mmm.ucar.edu/wrf/users/workshops/WS2016/oral_presentations/1.3.pdf.

[19] Alex Guenther, Russell K. Monson, and Ray Fall. Isoprene and monoterpene emission rate variability - observations with eucalyptus and emission rate algorithm development. *Journal of Geophysical Research: Atmospheres*, 96:10799–10808, 06 1991.

[20] Alex Guenther, Patrick R. Zimmerman, Peter C. Harley, Russell K. Monson, and Ray Fall. Isoprene and monoterpene emission rate variability: Model evaluations and sensitivity analyses. *Journal of Geophysical Research: Atmospheres*, 98(D7):12609–12617, 1993.

[21] Alex Guenther, Patrick Zimmerman, and Mary Wildermuth. Natural volatile organic compound emission rate estimates for u.s. woodland landscapes. *Atmospheric Environment*, 28(6):1197 – 1210, 1994.

[22] Hogrefe C., Lynn B., Civerolo K., Ku J.-Y., Rosenthal J., Rosenzweig C., Goldberg R., Gaffin S., Knowlton K., and Kinney P. L. Simulating changes in regional air pollution over the eastern united states due to changes in global and regional climate and emissions. *Journal of Geophysical Research: Atmospheres*, 109(D22).

[23] Song-You Hong, Yign Noh, and Jimy Dudhia. A new vertical diffusion package with an explicit treatment of entrainment processes. *Monthly Weather Review*, 134(9):2318–2341, 2006.

[24] G. Huang, R. Brook, M. Crippa, G. Janssens-Maenhout, C. Schieberle, C. Dore, D. Guizzardi, M. Muntean, E. Schaaf, and R. Friedrich. Speciation of anthropogenic emissions of non-methane volatile organic compounds: a global gridded data set for 1970–2012. *Atmospheric Chemistry and Physics*, 17(12):7683–7701, 2017.

[25] Michael J. Iacono, Jennifer S. Delamere, Eli J. Mlawer, Mark W. Shephard, Shepard A. Clough, and William D. Collins. Radiative forcing by long-lived greenhouse gases: Calculations with the aer radiative transfer models. *Journal of Geophysical Research: Atmospheres*, 113(D13), 2008.

[26] Daniel J. Jacob and Darrell A. Winner. Effect of climate change on air quality. *Atmospheric Environment*, 43(1):51 – 63, 2009. Atmospheric Environment - Fifty Years of Endeavour.

[27] Stijn Janssen, Cristina Guerreiro, Peter Viaene, Emilia Georgieva, and Philippe Thunis. *Guidance Document on Modelling Quality Objectives and Benchmarking*. FAIRMODE, 2017. http://fairmode.jrc.ec.europa.eu/downloads.html.

[28] J. Karlický, P. Huszár, and T. Halenka. Validation of gas phase chemistry in the wrf-chem model over europe. *Advances in Science and Research*, 14:181–186, 2017.

[29] Klea Katsouyanni, Jonathan M Samet, H Ross Anderson, Richard Atkinson, Alain Le Tertre, Sylvia Medina, Evangelia Samoli, Giota Touloumi, Richard T Burnett, Daniel Krewski, Timothy Ramsay, Francesca Dominici, Roger D Peng, Joel Schwartz, and Antonella Zanobetti. *Air Pollution and Health: A European and North American Approach*. Health Effects Institute, 2009.

[30] Nelson A. Kelly, Martin A. Ferman, and George T. Wolff. The chemical and meteorological conditions associated with high and low ozone concentrations in southeastern michigan and nearby areas of ontario. *Journal of the Air Pollution Control Association*, 36(2):150–158, 1986.

[31] Yuh-Lang Lin, Richard D. Farley, and Harold D. Orville. Bulk parameterization of the snow field in a cloud model. *Journal of Climate and Applied Meteorology*, 22(6):1065–1092, 1983.

[32] Eli J. Mlawer, Steven J. Taubman, Patrick D. Brown, Michael J. Iacono, and Shepard A. Clough. Radiative transfer for inhomogeneous atmospheres: Rrtm, a validated correlated-k model for the longwave. *Journal of Geophysical Research: Atmospheres*, 102(D14):16663–16682, 1997.

[33] National Research Council. *Rethinking the Ozone Problem in Urban and Regional Air Pollution*. The National Academies Press, Washington, DC, 1991.

[34] NCEP/NCDC. GFS model datasets. https://www.ncdc.noaa.gov/data-access/model-data/model-datasets/global-forcast-system-gfs.

[35] OECD. *OECD Environmental Outlook to 2050*. 2012.

[36] Ashley Penrod, Yang Zhang, Kai Wang, Shiang-Yuh Wu, and L. Ruby Leung. Impacts of future climate and emission changes on U.S. air quality. *Atmospheric Environment*, 89:533 – 547, 2014.

[37] PORG. *Ozone in the United Kingdom: Fourth report of the UK photochemical oxidants review group*. London, Department of the Environment, Transport and the Regions, 1997.

[38] V. Ramanathan, L. Callis, R. Cess, J. Hansen, I. Isaksen, W. Kuhn, A. Lacis, F. Luther, J. Mahlman, R. Reck, and M. Schlesinger. Climate-chemical interactions and effects of changing atmospheric trace gases. *Rev. Geophys.*, 25:1441–1482, 1987.

[39] Keywan Riahi, Arnulf Grübler, and Nebojsa Nakicenovic. Scenarios of long-term socio-economic and environmental development under climate stabilization. *Technological Forecasting and Social Change*, 74(7):887 – 935, 2007. Greenhouse Gases - Integrated Assessment.

[40] Jerry D. Rogers. Ultraviolet absorption cross sections and atmospheric photodissociation rate constants of formaldehyde. *The Journal of Physical Chemistry*, 94(10):4011–4015, 1990.

[41] RTI. *Investigation Of Rural Oxidants Levels As Related To Urban Hydro Carbon Control Strategies*. 1975. https://nepis.epa.gov/Exe/ZyPURL.cgi?Dockey=20015E5G.txt.

[42] Suranjana Saha, Shrinivas Moorthi, Hua-Lu Pan, Xingren Wu, Jiande Wang, Sudhir Nadiga, Patrick Tripp, Robert Kistler, John Woollen, David Behringer, Haixia Liu, Diane Stokes, Robert Grumbine, George Gayno, Jun Wang, Yu-Tai Hou, Hui ya Chuang, Hann-Ming H. Juang, Joe Sela, Mark Iredell, Russ Treadon, Daryl Kleist, Paul Van Delst, Dennis Keyser, John Derber, Michael Ek, Jesse Meng, Helin Wei, Rongqian Yang, Stephen Lord, Huug van den Dool, Arun Kumar, Wanqiu Wang, Craig Long, Muthuvel Chelliah, Yan Xue, Boyin Huang, Jae-Kyung Schemm, Wesley Ebisuzaki, Roger Lin, Pingping Xie, Mingyue Chen, Shuntai Zhou, Wayne Higgins, Cheng-Zhi Zou, Quanhua Liu, Yong Chen, Yong Han, Lidia Cucurull, Richard W. Reynolds, Glenn Rutledge, and Mitch Goldberg. The ncep climate forecast system reanalysis. *Bulletin of the American Meteorological Society*, 91(8):1015–1058, 2010.

[43] Erika von Schneidemesser, Paul S. Monks, James D. Allan, Lori Bruhwiler, Piers Forster, David Fowler, Axel Lauer, William T. Morgan, Pauli Paasonen, Mattia Righi, Katerina Sindelarova, and Mark A. Sutton. Chemistry and the linkages between air quality and climate change. *Chemical Reviews*, 115(10):3856–3897, 2015.

[44] E. von Schneidemesser, J. Coates, H.A.C. Denier van der Gon, A.J.H. Visschedijk, and T.M. Butler. Variation of the NMVOC speciation in the solvent sector and the sensitivity of modelled tropospheric ozone. *Atmospheric Environment*, 135:59 – 72, 2016.

[45] John H. Seinfeld and Spyros N. Pandis. *Atmospheric Chemistry and Physics: From Air Pollution to Climate Change*. John Wiley and Sons, Inc, 1998.

[46] S. Sillman and P.J. Samson. Impact of temperature on oxidant photochemistry in urban, polluted rural and remote environments. *Journal of Geophysical Research: Atmospheres*, 100(D6):11497–11508, 1995.

[47] Sanford Sillman and Dongyang He. Some theoretical results concerning o3-nox-voc chemistry and nox-voc indicators. *Journal of Geophysical Research*, 107, 11 2002.

[48] Sanford Sillman. Overview: Tropospheric ozone, smog and ozone-nox-voc sensitivity. http://www-personal.umich.edu/~sillman/Sillman-webOZONE.pdf, 2003. Accessed: 2018-04-25.

[49] D. Simpson, A. Guenther, C.N. Hewitt, and R. Steinbrecher. Biogenic emissions in europe: 1. estimates and uncertainties. *Journal of Geophysical Research: Atmospheres*, 100(D11):22875–22890, 1995.

[50] W.R. Stockwell, P. Middleton, J.S. Chang, and X. Tang. The second generation regional acid deposition model chemical mechanism for regional air quality modeling. *Journal of Geophysical Research: Atmospheres*, 95(D10):16343–16367, 1990.

[51] Efthimios Tagaris, Kasemsan Manomaiphiboon, Kuo-Jen Liao, L. Ruby Leung, Jung-Hun Woo, Shan He, Praveen Amar, and Armistead G. Russell. Impacts of global

climate change and emissions on regional ozone and fine particulate matter concentrations over the united states. *Journal of Geophysical Research: Atmospheres*, 112(D14).

[52] M Tewari, F Chen, W Wang, Jimy Dudhia, M.A. LeMone, Kieran Mitchell, M Ek, G Gayno, Jerry Wegiel, and Richard Cuenca. Implementation and verification of the united noah land surface model in the wrf model. *20th Conference on Weather Analysis and Forecasting/16th Conference on Numerical Weather Prediction*, pages 11–15, 2004.

[53] Thornton, J. Acyl peroxy nitrates: Importance and detection. https://atmos.washington.edu/~thornton/PANs.html, 2007. Accessed: 2018-04-24.

[54] P. Thunis, D. Pernigotti, and M. Gerboles. Model quality objectives based on measurement uncertainty. part i: Ozone. *Atmospheric Environment*, 79:861 – 868, 2013.

[55] G. Tripepi, K.J. Jager, F.W. Dekker, C. Wanner, and C. Zoccali. Measures of effect: Relative risks, odds ratios, risk difference, and 'number needed to treat'. *Kidney International*, 72(7):789 – 791, 2007.

[56] Daniel Vallero. Chapter 2 - the physics of the atmosphere. In *Fundamentals of Air Pollution (Fifth Edition)*, pages 23 – 42. Academic Press, Boston, fifth edition edition, 2014.

[57] D. J. Wackter and P.V. Bayly. The effectiveness of emission controls on reducing ozone levels in connecticut from 1976 through 1987. In *The Scientific and Technical Issues Facing Post-1987 Ozone Control Strategies: A Conference Summary*, pages 398–415, 1988.

[58] C. P. Weaver, X.-Z. Liang, J. Zhu, P. J. Adams, P. Amar, J. Avise, M. Caughey, J. Chen, R. C. Cohen, E. Cooter, J. P. Dawson, R. Gilliam, A. Gilliland, A. H. Goldstein, A. Grambsch, D. Grano, A. Guenther, W. I. Gustafson, R. A. Harley, S. He, B. Hemming, C. Hogrefe, H.-C. Huang, S. W. Hunt, D.J. Jacob, P. L. Kinney, K. Kunkel, J.-F. Lamarque, B. Lamb, N. K. Larkin, L. R. Leung, K.-J. Liao, J.-T. Lin, B. H. Lynn, K. Manomaiphiboon, C. Mass, D. McKenzie, L. J. Mickley, S. M. O'neill, C. Nolte, S. N. Pandis, P. N. Racherla, C. Rosenzweig, A. G. Russell, E. Salathé, A. L. Steiner, E. Tagaris, Z. Tao, S. Tonse, C. Wiedinmyer, A. Williams, D. A. Winner, J.-H. Woo, S. WU, and D. J. Wuebbles. A Preliminary Synthesis of Modeled Climate Change Impacts on U.S. Regional Ozone Concentrations. *Bulletin of the American Meteorological Society*, 90(12):1843–1864, 2009.

[59] M.L. Wesely. Parameterization of surface resistances to gaseous dry deposition in regional-scale numerical models. *Atmospheric Environment (1967)*, 23(6):1293 – 1304, 1989.

[60] WHO. *WHO Air quality guidelines for particulate matter, ozone, nitrogen dioxide and sulfur dioxide*. World Health Organization, 2005.

[61] WHO. *Health risks of air pollution in Europe – HRAPIE project*. World Health Organization - Regional office for Europe, 2013.

[62] WHO. *WHO Air Pollution homepage*. World Health Organization, 2018. Accessed 13 June 2018.

[63] Rahul A. Zaveri and Leonard K. Peters. A new lumped structure photochemical mechanism for large-scale applications. *Journal of Geophysical Research: Atmospheres*, 104(D23):30387–30415, 1999.

[64] Detlef P. van Vuuren, Michel G. J. den Elzen, Paul L. Lucas, Bas Eickhout, Bart J. Strengers, Bas van Ruijven, Steven Wonink, and Roy van Houdt. Stabilizing greenhouse gas concentrations at low levels: an assessment of reduction strategies and costs. *Climatic Change*, 81(2):119–159, Mar 2007.

Appendix - Population exposures to excessive ozone concentrations

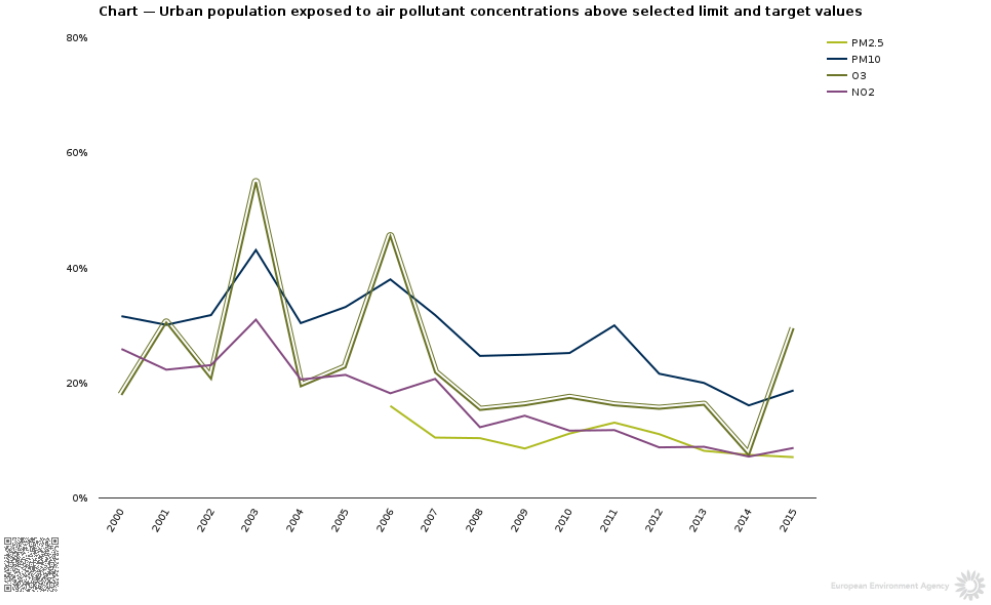

Figure 22: Percentage of Europe's urban population exposed to ozone concentrations (yellow line) that exceed the EU limit value (120 μg m^{-3} more than 25 days per year).

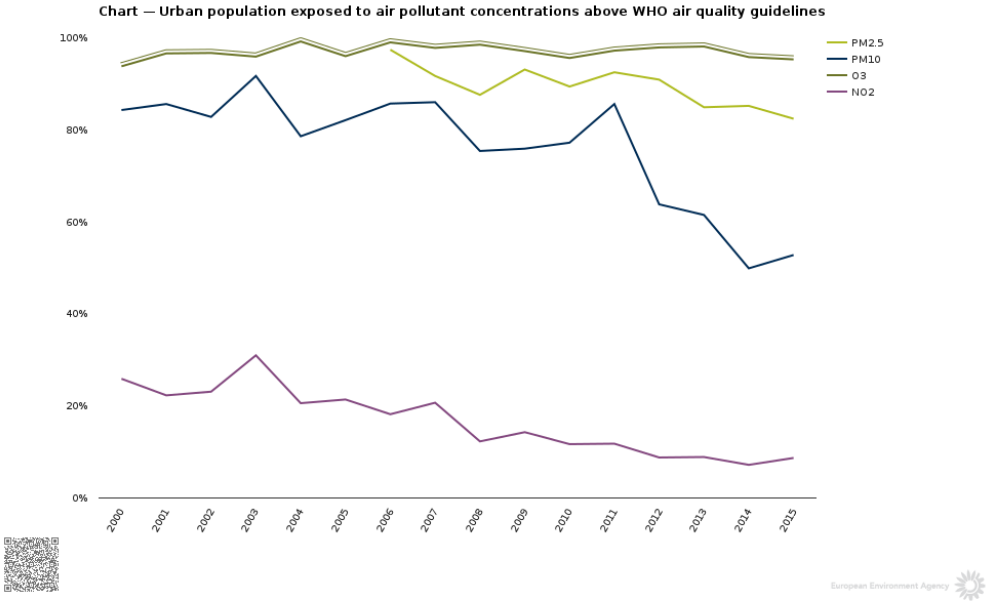

Figure 23: Percentage of Europe's urban population exposed to ozone concentrations (yellow line) that exceed the WHO limit value (100 μg m^{-3}).